Measurements of NO, NOy, N2O, and O3 during SPURT: implications for transport and chemistry in the lowermost stratosphere

M. I. Hegglin, D. Brunner, T. Peter, P. Hoor, H. Fischer, J. Staehelin, M. Krebsbach, C. Schiller, U. Parchatka, U. Weers

**Atmospheric
Chemistry
and Physics**

Measurements of NO, NO$_y$, N$_2$O, and O$_3$ during SPURT: implications for transport and chemistry in the lowermost stratosphere

M. I. Hegglin[1,*], **D. Brunner**[1], **T. Peter**[1], **P. Hoor**[2], **H. Fischer**[2], **J. Staehelin**[1], **M. Krebsbach**[3], **C. Schiller**[3], **U. Parchatka**[2], **and U. Weers**[1]

[1]Institute for Atmospheric and Climate Science, Swiss Federal Institute of Technology, Zurich, Switzerland
[2]Max Planck Institute for Chemistry, Air Chemistry, Mainz, Germany
[3]Institute for Chemistry and Dynamics of the Geosphere: Stratosphere, Research Centre Jülich GmbH, Jülich, Germany
[*]now at: Department of Physics, University of Toronto, Toronto, Canada

Abstract. We present measurements of NO, NO$_y$, O$_3$, and N$_2$O within the lowermost stratosphere (LMS) over Europe obtained during the SPURT project. The measurements cover all seasons between November 2001 and July 2003. They span a broad band of latitudes from 30° N to 75° N and a potential temperature range from 290 to 380 K. The measurements represent a comprehensive data set of these tracers and reveal atmospheric transport processes that influence tracer distributions in the LMS. Median mixing ratios of stratospheric tracers in equivalent latitude-potential temperature coordinates show a clear seasonal cycle related to the Brewer-Dobson circulation, with highest values in spring and lowest values in autumn. Vertical tracer profiles show strong gradients at the extratropical tropopause, suggesting that vertical (cross-isentropic) mixing is reduced above the tropopause. Pronounced meridional gradients in the tracer mixing ratios are found on potential temperature surfaces in the LMS. This suggests strongly reduced mixing along isentropes. Concurrent large gradients in static stability in the vertical direction, and of PV in the meridional direction, suggest the presence of a mixing barrier. Seasonal cycles were found in the correlation slopes ΔO$_3$/ΔN$_2$O and ΔNO$_y$/ΔN$_2$O well above the tropopause. Absolute slope values are smallest in spring indicating chemically aged stratospheric air originating from high altitudes and latitudes. Larger values were measured in summer and autumn suggesting that a substantial fraction of air takes a "short-cut" from the tropical tropopause region into the extratropical LMS. The seasonal change in the composition of the LMS has direct implications for the ozone chemistry in this re-

gion. Comparisons of measured NO with the critical NO value at which net ozone production changes from negative to positive, imply ozone production up to 20 K above the local tropopause in spring, up to 30 K in summer, and up to 40 K in autumn. Above these heights, and in winter, net ozone production is negative.

1 Introduction

Ozone concentrations in the upper troposphere/lowermost stratosphere (UT/LMS) are known to have a strong radiative influence on surface temperatures (Lacis et al., 1990; Forster and Shine, 1997). In the UT/LMS, ozone is a long lived species and its concentration is affected by both transport and in situ chemistry. Measurements of long-lived species, and short-lived ozone precursors, are needed to improve our understanding of the current UT/LMS ozone budget, and how it may evolve in the future.

Reactive nitrogen (NO$_y$) plays a key role in ozone chemistry via both gas-phase and heterogeneous reactions. Above about 18 km, catalytic cycles involving NO$_x$ (=NO+NO$_2$) destroy ozone. In the troposphere and LMS NO$_x$ acts together with hydrocarbons and carbon monoxide to produce ozone (IPCC, 1999). Although there are fewer measurements within the UT/LMS, ozone chemistry within this region can be expected to be intermediate between these two regimes. Climatologies of NO$_y$, NO$_x$, and other atmospheric key species involved in ozone chemistry have been obtained from satellite measurements and passenger aircraft. However, these measurements lack vertical resolution and accuracy in the tropopause region, or have occurred over a limited

altitude range. A tropospheric climatology has been compiled from 30 aircraft campaigns between 1983 and 1996 (Emmons et al., 2000). More recent measurements were presented by Kondo et al. (1997), Singh et al. (1997), Ziereis et al. (2000), and Baehr et al. (2003). The first observations of NO$_x$ and O$_3$ in the UT/LMS of the Northern hemisphere on a regular basis were collected during the Swiss NOXAR and the European POLINAT-2 projects using a commercial aircraft as measurement platform (Brunner et al., 2001). O$_3$ and NO$_y$ are measured by MOZAIC since 1994 and 2001, respectively (Volz-Thomas et al., 2005). Strahan et al. (1999a, b) presented a climatology of stratospheric NO$_y$, O$_3$, and N$_2$O between potential temperatures of 360 K and 530 K. Their measurements reveal the effects of dynamical features such as transport barriers, and the global mean circulation, on the distributions of these long-lived trace gas species.

The main source of NO$_y$ in the stratosphere is N$_2$O oxidiation. Other sources of NO$_y$ in the LMS include aircraft emissions, and potentially, the deep convective injection of polluted planetary boundary layer air or of air affected by lightning (Hegglin et al., 2004, and references therein). In general, tracer distributions in the LMS will therefore be influenced by both the residual meridional circulation (or Brewer-Dobson circulation) and extratropical stratosphere-troposphere exchange (STE) (Holton et al., 1995). Climatological studies, e.g. those using Lagrangian model approaches, have led to improvements in our understanding of the seasonality, spatial distribution, and magnitude of STE (Wernli and Bourqui, 2002; Sprenger and Wernli, 2003; James et al., 2003). Further improvements in our understanding of the degree to which STE leads to irreversible mixing and how it influences the vertical and latitudinal distribution of trace gas species, will require additional measurements of trace gases. Vertical profiles of CO measured during SPURT have revealed the existence of a mixing layer extending up to 20 or 30 K above the local dynamical tropopause during all seasons (Hoor et al., 2004). The chemical composition of this mixing layer exhibits characteristics of both the troposphere and the stratosphere. However, the impact of STE on the distribution of a particular trace gas species in the UT/LMS will also be influenced by the source/sink characteristics, and possibly microphysics, of the species. A tropospheric tracer which is well-mixed in the troposphere, such as N$_2$O or CO, is likely to show less variability than one with localized sources and sinks (e.g. NO$_y$ and H$_2$O).

Here we present high resolution and high sensitivity airborne data of NO, NO$_y$, N$_2$O, and O$_3$. These were obtained during eight seasonally conducted measurement campaigns focusing on the LMS region up to 13.7 km, each part of the project SPURT (German: SPURenstofftransport in der Tropopausenregion). The data reveal new information about the seasonal distributions of the measured trace gas species and represent a valuable contribution to the existing climatology between the tropopause and $\Theta=380$ K (Θ–potential temperature). This paper is part of a SPURT special issue,

in which other tracer data together with tracer-specific evaluations are presented. An overview of the SPURT project is provided by Engel et al. (2006).

A short description of the measurement systems used, and their performance and overall accuracy is given in Sect. 2. Section 3 describes the evaluation methods. Section 4.1 presents median tracer distributions in equivalent latitude – potential temperature coordinates most suited to be used as diagnostics for the validation of chemical transport models (CTMs) and global circulation models (GCMs). Section 4.2 discusses the role of the tropopause in shaping tracer distributions. Section 4.3 shows tracer-tracer correlations which give insight into the seasonal variability of the Brewer Dobson circulation. Finally, in Sect. 4.4, we present a new calculation of the critical NO mixing ratio (NO$_{crit}$) at which O$_3$ production changes from positive to negative. This calculation takes into account both the tropospheric and the stratospheric characteristics of the LMS.

2 Chemical measurements

There was a total of 36 flights during SPURT. Each flight provided between 3 and 5 h of data. The flights covered a latitudinal range from 30° N to 75° N over Europe. The measurement platform was a Learjet 35A, which can reach flight altitudes up to 13.7 km.

NO$_y$, NO, and O$_3$ were measured using a three channel chemiluminescence detector ECO-Physics CLD 790-SR for fast and highly sensitive measurements, in the following termed "ECO". The measurement principle is based on chemiluminescence obtained in the reaction between NO and O$_3$ yielding NO$_2$ in an electronically excited state (Fontijn et al., 1970). Relaxation occurs through quenching and partly through emission of light. If one reactant is supplied in excess, then the light intensity is proportional to the volume mixing ratio of the other reactant. Following this principle, NO is measured by adding an excess of O$_3$, while O$_3$ is measured by using an excess of NO as reactant.

Total reactive nitrogen (NO$_y$=NO+NO$_2$+NO$_3$+HNO$_3$ +HNO$_4$+HONO+PAN+ RONO$_2$+ClONO$_2$+2×N$_2$O$_5$ +BrONO$_2$+ organic nitrate + particulate nitrate (<1 μm)) was measured by chemiluminescence after reducing NO$_y$ species to NO by means of an externally mounted catalytic gold converter with CO as reduction agent (Fahey et al., 1985). The converter samples in backward direction in order to exclude particles with diameter >1 μm. For technical details of the converter see Lange et al. (2002).

The conversion efficiency of the analyzer was quantified using gas phase titration (GPT) of NO with O$_3$ to produce NO$_2$ before and after each campaign. With the exception of the first campaign (Hegglin et al., 2004), the conversion efficiency did not significantly change over the 7 days of a campaign and varied between 95% and 98%. The sensitivities of the NO and NO$_y$ channels were calibrated twice during

the flight by adding known amounts of NO (Sauerstoffwerk Lenzburg AG: 9.4 ppm$\pm$2% NO in N$_2$) showing that its sensitivity varied by less than 3.5%. The chemiluminescence detector was switched every 2 min for 10 s to pre-chamber mode in order to determine the instrument background signal (Ridley and Howlett, 1974). In addition, zero calibrations with synthetic air were performed three times during each flight to determine the temporal evolution of the NO$_y$ artifact signal which is a common feature in NO$_y$ measurements. Its origin is not fully understood but is in part due to impurities of the CO reduction agent (Fahey et al., 1985). A possible error in accounting for the NO$_y$ artifact signal may introduce an offset of maximal 20 to 50 pptv to the data. Note that the specific design of the converter allows the addition of all calibration gases upstream of the converter at the inlet tip. An Advanced Pollution Instrumentation (API) UV photometric ozone calibrator was used as transfer standard for calibration of the O$_3$-channel on ground.

The precision of the NO$_y$, NO and O$_3$ data with a resolution of 1 Hz was determined from the fluctuations of the background signal. The accuracy was calculated by taking into account the uncertainties in the calibration gas standards ($\pm$4%) and the variation of the mass flow controllers ($\pm$2%). For the NO$_y$-channel the accuracy contains also the uncertainties in the conversion efficiency for different species ($\pm$10%), an additional calibration gas uncertainty of ($\pm$3.7%), the reproducibility of the conversion efficiency experiments ($\pm$3%) and an experimentally determined pressure correction ($\pm$4%). The overall accuracies of the NO$_y$, NO and O$_3$ then are $\pm$(0.126$\cdot$[NO$_y$]+11 pptv), $\pm$(0.045$\cdot$[NO]+9 pptv), and $\pm$(0.05$\cdot$[O$_3$]+149 pptv), respectively. These specifications refer to a 2σ confidence level (σ is the standard deviation).

The NO$_y$ measurement of ECO was compared side-by-side with the NO$_y$ instrument used in the EU program MOZAIC (Pätz et al., 2006) temporally mounted on the Learjet during a dedicated instrument validation flight. The two systems agree within 6% with some deviations after calibration and during ascent and descent phases of the aircraft where the differences lie outside the range of the combined stated accuracies.

During the November 2001 and the January 2002 campaigns, an older 1-channel measurement system was used which measured NO$_y$ only. O$_3$ from the Jülich Ozone Experiment JOE with an accuracy of 5% (Mottaghy, 2001) is shown for these two campaigns, while NO$_x$ (=NO+NO$_2$) data are missing. Ozone from the JOE and the ECO analyzers agree to within 6.4% for the ozone measurements during the other SPURT campaigns (Hegglin, 2004; Engel et al., 2006).

N$_2$O data was measured with a Tunable Diode Laser Absorption Spectrometer (TDLAS), which has a total uncertainty of less than $\pm$2% (Hoor et al., 2002).
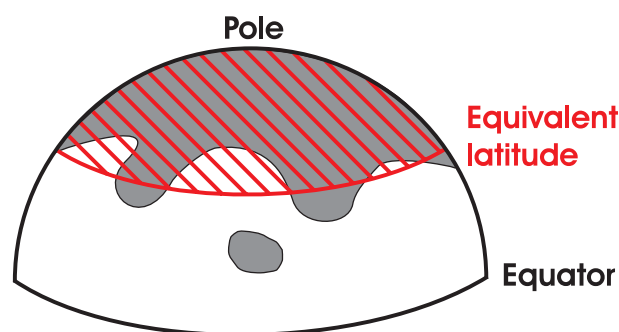
Fig. 1. Sketch illustrating the concept of equivalent latitude (ϕ_e). An area (grey colored) enclosed by a PV-contour on a given isentrope is transformed into a circle centered about the pole of equal area (red hatched). The latitude of this circle is defined as ϕ_e. By using its ϕ_e, a cut-off low with high PV at mid-latitudes and on a given isentrope is moved back to higher latitudes.

3 Methods

3.1 Equivalent latitude-potential temperature coordinates

Rossby and smaller scale waves lead to deviations of the local tropopause from the climatological mean. The associated north-south excursions of air parcels are adiabatic to first order and largely reversible. They lead to large variability in trace gas distributions in a geometric (longitude, latitude, pressure) coordinate system, since chemical constituents are advected from regions with higher or lower climatological mean concentrations at the same time. In an attempt to remove this variability we therefore use a two-dimensional potential vorticity based equivalent latitude (ϕ_e) and potential temperature (Θ) framework to present our data. This framework follows the meridional deformations in PV contours and uses the fact that PV behaves like a passive tracer under adiabatic and frictionless motions. The equivalent latitude of a PV contour is defined as the latitude of a circle centered about the pole enclosing the same area as the PV contour (Butchart and Remsberg, 1986). This is illustrated in Fig. 1. If A(PV) is the area enclosed by the PV contour, then its equivalent latitude is given by ϕ_e (PV)=sin^{-1} (1- A(PV) / (2πr$_e^2$)). For the SPURT measurements the PV-equivalent latitude relationships were calculated for 27 individual isentropes from Θ=270 K up to Θ=400 K in steps of 5 K. In this way we obtained a field ϕ_e(PV, Θ) for discrete values of PV and Θ. The equivalent latitude for each measurement point was then calculated by bilinear interpolation onto [PV(t),Θ(t)]. PV(t) and Θ(t) are obtained from a combination of 6-hourly analyses and 3-hourly forecast ECMWF model fields interpolated in space and time onto the flight track [lon(t), lat(t), p(t)]. Since equivalent latitude is a PV coordinate, its calculation relies on monotonically increasing PV values. A recent study by Birner (2006) found that PV in the UT/LMS exhibits only small meridional gradients away

from the tropopause. An interpretation regarding geographical dependencies of tracers based on the equivalent latitude framework should therefore be treated carefully in regions away from the tropopause. However, Hegglin et al. (2005) used the equivalent latitude-potential temperature framework in a 2-D advection-diffusion model to simulate tracer distributions in the LMS and obtained correlation coefficients (R^2) between 0.72 and 0.94 between modeled and observed carbon monoxide mixing ratios.

3.2 Vertical tracer profiles

The vertical distribution of a trace gas species is also strongly influenced by the meteorological situation and in particular by the actual position of the tropopause. The altitude of the tropopause can vary by several kilometers. Because conventional averaging in altitude can smear out vertical structures in chemical species associated with the tropopause, it is desirable to plot chemical species relative to the actual tropopause height. For this purpose, we use the difference between the potential temperature at flight level and at the tropopause ($\Delta\Theta$). The potential temperature of the tropopause was calculated from ECMWF data. The tropopause is defined here as the 2 PVU surface (with 1 PVU=10^{-6} m^2 s^{-1} K kg^{-1}). The use of $\Delta\Theta$ as the vertical coordinate reduces scatter and increases compactness in tracer profiles as compared with using absolute potential temperature values (Hoor et al., 2004). Pan et al. (2004) found a similar result by using distance (in km) relative to the thermal tropopause.

3.3 Tracer-tracer correlations

The theoretical framework of the relation between long-lived stratospheric tracers has been provided by Plumb and Ko (1992). They showed that the combination of quasi-horizontal mixing along isentropes and differential vertical advection (upwards in the tropics and downwards in polar regions) cause tracer isopleths to slope relative to the isentropes. Since this shape is shared by different long-lived species, scatter plots of two such tracers form linear correlations. Tracer-tracer correlations since then have been demonstrated to serve as valuable tools for the study of transport processes in the stratosphere and for the validation of CTMs (Bregman et al., 2000) or GCMs (Sankey and Shepherd, 2003). The use of a chemical framework removes much of the variability found in tracer time series which are caused by advection of air masses (because different long-lived tracers are advected similarly). This is similar to the equivalent-latitude concept. In this study we focus on the correlations between NO$_y$ and N$_2$O, O$_3$ and N$_2$O, and NO$_y$ and O$_3$.

NO$_y$ is predominantly produced in the tropical lower stratosphere by the oxidation reaction

$$N_2O + O(^1D) \rightarrow NO + NO \tag{1}$$

which accounts for 5.8% of the total N$_2$O loss. Highest production rates for NO$_y$ are found in the tropical stratosphere between 25 and 35 km. Since photochemistry is also involved in the production of O$_3$ in this region, NO$_y$ and O$_3$ are positively correlated with each other. In contrast N$_2$O is a tropospheric tracer which only has a sink in the stratosphere by photolysis and the reaction with O(^{1}D). It is therefore negatively correlated with both, NO$_y$ and O$_3$. Above 40 km, NO$_y$ loss becomes important due to the reaction

$$NO + N \rightarrow N_2 + O \tag{2}$$

and NO$_y$ becomes positively correlated with N$_2$O. Also the correlation between N$_2$O and O$_3$ becomes positive as one exceeds the O$_3$ maximum above around 30 km. Due to chemical aging during transport towards the poles and mixing with air masses originating from above the O$_3$ and NO$_y$ maxima, the slopes of the tracer correlations $\Delta O_3/\Delta N_2O$ and $\Delta NO_y/\Delta N_2O$ show a latitudinal dependency with larger absolute values in the tropics than at the poles, and intermediate slopes in the mid-latitudinal surf-zone (Bregman et al., 2000; Proffitt et al., 2003). Tracer correlations between O$_3$ and N$_2$O, or between NO$_y$ and N$_2$O, and other long-lived species, have been widely used to estimate chemical ozone loss, to identify denitrification processes, and to characterize air mass origin (Proffitt et al., 2003, and references therein). However, the tracer-tracer correlations discussed here may not be an appropriate tool to identify chemical ozone loss. These correlations can be strongly influenced by the transport of chemically aged stratospheric air from above the O$_3$ or NO$_y$ maxima, or by mixing with stratospheric mid-latitudes air with different correlation-characteristics (Michelsen et al., 1998; Plumb et al., 2000). The SPURT data set offers the opportunity to obtain a seasonally and latitudinally resolved picture of the relationships between different long-lived tracers in the LMS. One issue is whether the linearity and compactness of the tracer-tracer correlations observed in the lower stratosphere is maintained in the LMS, or is instead modified by STE. The degree to which these linear correlations are maintained in the LMS may be useful in identifying transport pathways to this region, or reflect chemical processing.

3.4 Calculation of NO$_x$

The SPURT instrumentation just allowed the measurement of NO. Since NO converts rapidly into NO$_2$ and since both these species play an important role in the production and destruction of O$_3$ they are mostly treated as one species and denoted with NO$_x$. NO$_2$ can been calculated from the SPURT NO and O$_3$ mixing ratios using the photostationary equilibrium assumption by Crawford et al. (1996):

$$\frac{[NO]}{[NO_2]} = \frac{J_{NO_2}}{k_1 \cdot [O_3]} \tag{3}$$
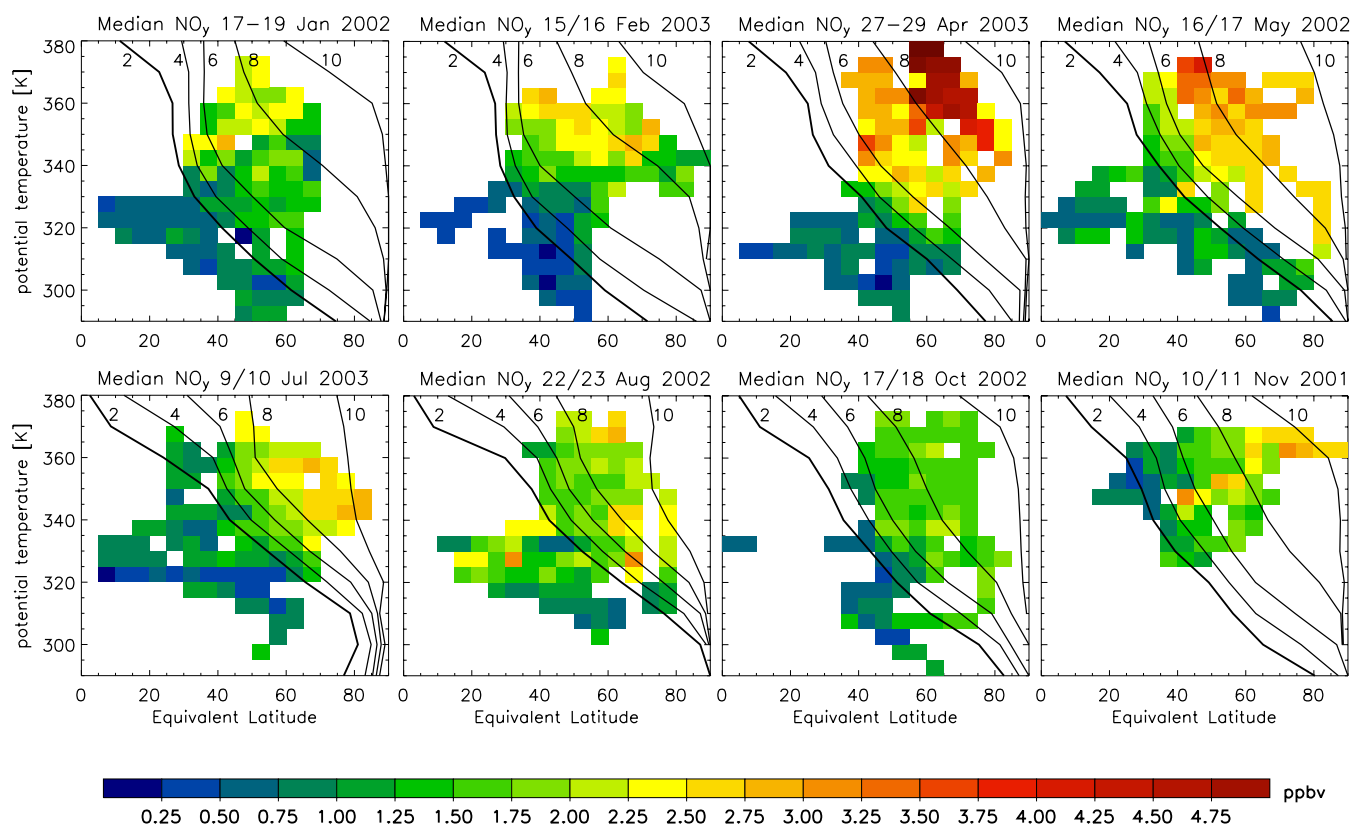
Fig. 2. Median NO$_y$ mixing ratios in (ϕ_e,Θ) coordinates. Black lines denote PV-isolines (2, 4, 6, 8, and 10 PVU). The contour with 2 PVU indicates the dynamical tropopause.

with J_{NO_2} being the photolysis rate of NO$_2$ with dependency on altitude and solar zenith angle for clear-sky conditions. k_1 further is the reaction rate of

$$NO + O_3 \rightarrow NO_2 + O_2. \tag{4}$$

For flights during night time NO$_x$ can not be calculated. The lifetime of NO$_x$ in the tropopause region is around 8 days (Jaeglé et al., 1998).

4   Results and discussion

In the following we present the data of the long-lived tracers NO$_y$, N$_2$O, O$_3$ and of the shorter-lived NO$_x$ (calculated from measured NO) by using the above discussed reference systems: Median distributions in (ϕ_e,Θ)-space for each campaign separately, vertical profiles in $\Delta\Theta$ from the tropopause with focus on the seasonality in the observed trace gas species, and tracer-tracer correlations in order to explore their applicability in the LMS region and to gain insight into the origin of the probed air masses. Finally, the influence of the measured NO mixing ratios on the ozone chemistry is evaluated.

4.1   Median tracer distributions in (ϕ_e, Θ) coordinates

All measurement points are binned into 5° equivalent latitude by 5 K potential temperature bins. For each bin including more than 4 data points, median values were computed. Medians have been used since they are less sensitive to extreme values in a data set than mean values. For the longer lived species N$_2$O and O$_3$, mean and median distributions show no significant differences, while NO$_y$ and NO$_x$ due to localized sources and sinks show mean values which are often higher than median values. 70% of the bins for each campaign include more than 20 data points with a maximum of 600 and a mean of 150 data points per bin. Most of the bins with less than 20 data points are located in the troposphere. Figures 2, 3, 4, and 5 show the distributions of median NO$_y$, N$_2$O, O$_3$, and NO$_x$ values during each campaign sorted by month and season.

The (ϕ_e,Θ) plots divide tropospheric and stratospheric air masses and extend the effective geographical coverage obtained in each campaign. As shown in Figs. 2 to 5, the SPURT data set achieved a good coverage of the mid-latitude LMS between 35° N and 65° N and below 380 K in mainly every season. During spring campaigns, the best height coverage in $\Delta\Theta$ from the tropopause has been obtained. Due to
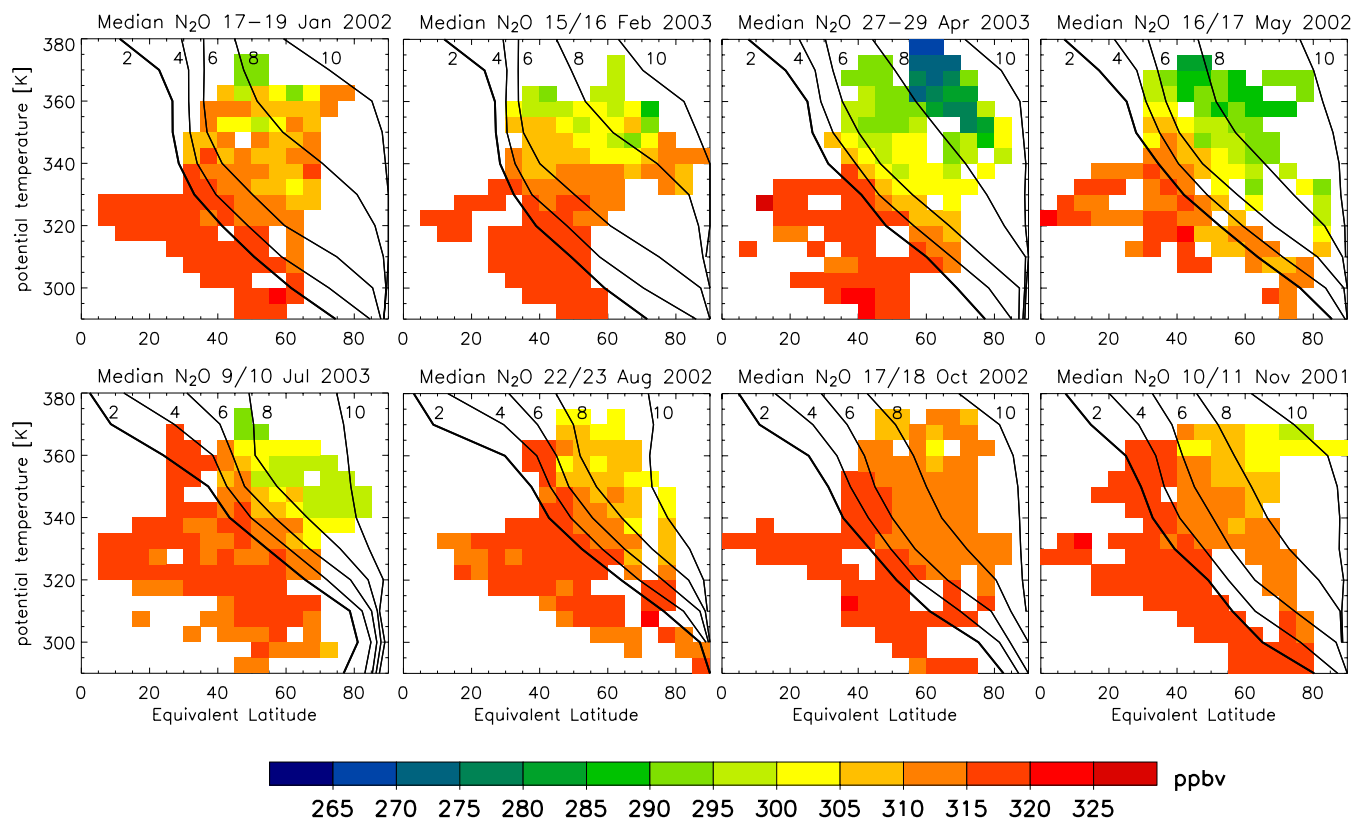
Fig. 3. Same as Fig. 2, but for N$_2$O.

instrument problems, only a few tropospheric measurements of NO$_y$ are available for the two autumn campaigns.

Campaigns conducted in different years may be considered as a sequence of months within one year (from January, February, April, May, July, August, October, to November) as shown in Figs. 2, 3, and 4. The result is a seasonal cycle in all of the tracer mixing ratios over the course of a year. Closer examination of single months reveal not only seasonal but also intra-seasonal differences present in the tracer distributions.

Highest NO$_y$ mixing ratios of around 5 ppbv, and O$_3$ of around 1000 ppbv, together with lowest N$_2$O of around 265 ppbv, are found in the LMS during the April campaign at highest Θ levels and PV-values between 8 and 10. These values decrease gradually towards autumn with a minimum in October, when tracer mixing ratios at these levels were around 2 ppbv NO$_y$ and 500 ppbv O$_3$. Simultaneously, N$_2$O values increased towards 310 ppbv.

The observed changes in the mixing ratios can be linked to the seasonality in the strength of the Brewer-Dobson circulation as follows. The stronger the mean meridional circulation, the more O$_3$ or NO$_y$ is transported from its source region in the tropical lower stratosphere towards higher latitudes and altitudes and then down into the LMS. Simultaneously, lowest N$_2$O mixing ratios are transported to the

LMS. However, the seasonal variation in the net mass flux across the 380 K isentrope and therefore in the strength of the Brewer-Dobson circulation exhibits a maximum in midwinter and a minimum in late spring/early summer (Appenzeller et al., 1996). We observe a shift of the maximum O$_3$ and NO$_y$ and the minimum N$_2$O mixing ratios towards April. This is due to the finite timescale of tracer transport from its source in the tropical stratosphere (above 380 K) to the LMS (below 380 K). The global mean circulation has been shown to dominate the seasonal cycle of long-lived trace gases in the lower stratosphere (Strahan et al., 1999a, b; Garcia et al., 1992). Our results show that this dominant influence extends down into the LMS. As will be discussed in Sect. 4.3 the influence of old stratospheric air is also dependent on the amount of relatively young air mixed from the tropical tropopause region to the mid-latitudes.

Tracer mixing ratios of O$_3$ and N$_2$O exhibit a strong gradient at the tropopause (with PV=2 PVU). The gradient is stronger pronounced in O$_3$ where tracer mixing ratios change from tropospheric values around 100 ppbv to stratospheric values of 500–800 ppbv. Corresponding changes in N$_2$O are from 318 ppbv in the troposphere to stratospheric values of 300 ppbv in autumn and 270 ppbv in spring. A gradient in the tracer mixing ratios across the tropopause is also seen in NO$_y$, although it shows higher variability in the
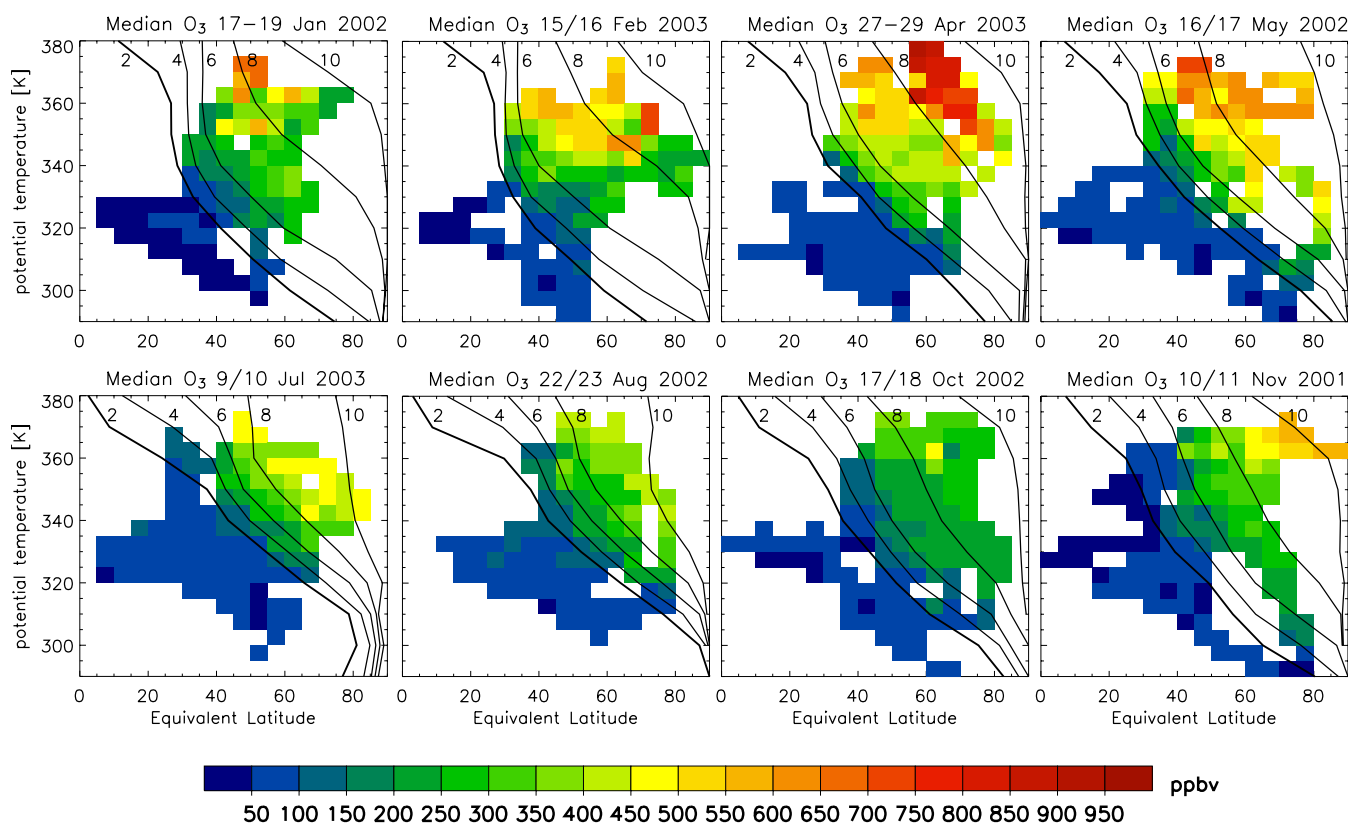
Fig. 4. Same as Fig. 2, but for O$_3$.

troposphere. The isopleths of the different tracers are closely following the shape of the tropopause similar to the SPURT CO-measurements (Hoor et al., 2004; Hegglin et al., 2005). With increasing PV, NO$_y$ and O$_3$ increase while N$_2$O decreases resulting in tight positive and negative correlations, respectively. A similar distribution along PV isolines was also found for H$_2$O (Krebsbach et al., 2006a, b[1]). However, the tracer isopleths are not strictly parallel to the PV-isolines, i.e. the correlations with PV are different on different isentropes. Furthermore, the relationship is strongly varying with season. Note that pronounced gradients in the tracer mixing ratios exist at the tropopause both across potential temperature levels and horizontally along isentropes. This implies that the extratropical tropopause acts as a barrier to transport and mixing in both, the vertical and the horizontal directions. Vertical transport through the tropopause is inhibited by a strong gradient in static stability, whereas quasi-horizontal transport along isentropes is inhibited by a strong meridional gradient in PV at the tropopause which can be seen in any of Figs. 2 to 5. Note, due to their low resolution, the use of ECMWF fields for the calculation of the equivalent lati-

tude may lead to a potential smearing out of the real tracer gradients at the tropopause. Nevertheless, it represents a major improvement towards the use of geometrical coordinates where tropospheric and stratospheric air masses are not separated before the averaging.

The shorter lived tracer NO$_x$, on the other hand, is much more variable as can be seen in Fig. 5. This is because it has many different local sources and sinks, a relatively short lifetime of about 8 days in the UT/LMS (Jaeglé et al., 1998), and a strong dependency on available sunlight. During the autumn and winter campaigns with little sunlight, NO$_x$ mixing ratios are around 0.1 ppbv. The calculation of NO$_x$ fails, as soon as no sunlight is available (cf. Sect. 3.4). During polar night, NO$_x$ is mainly converted into its reservoir species such as N$_2$O$_5$, HNO$_3$, or ClONO$_2$. In the presence of sunlight during spring and summer, however, NO$_x$ is reactivated which leads to generally higher mixing ratios with values around 0.3 ppbv. Patches in the observed distributions may be a result of relatively fresh sources of NO$_x$ transported into the LMS after production by lightning or convective uplift of emissions from the planetary boundary layer. These processes have the potential to alter significantly mean NO$_y$ mixing ratios (see Hegglin et al., 2004). Aircraft emissions are another relevant source of NO$_x$ in the mid-latitudinal LMS over Europe.
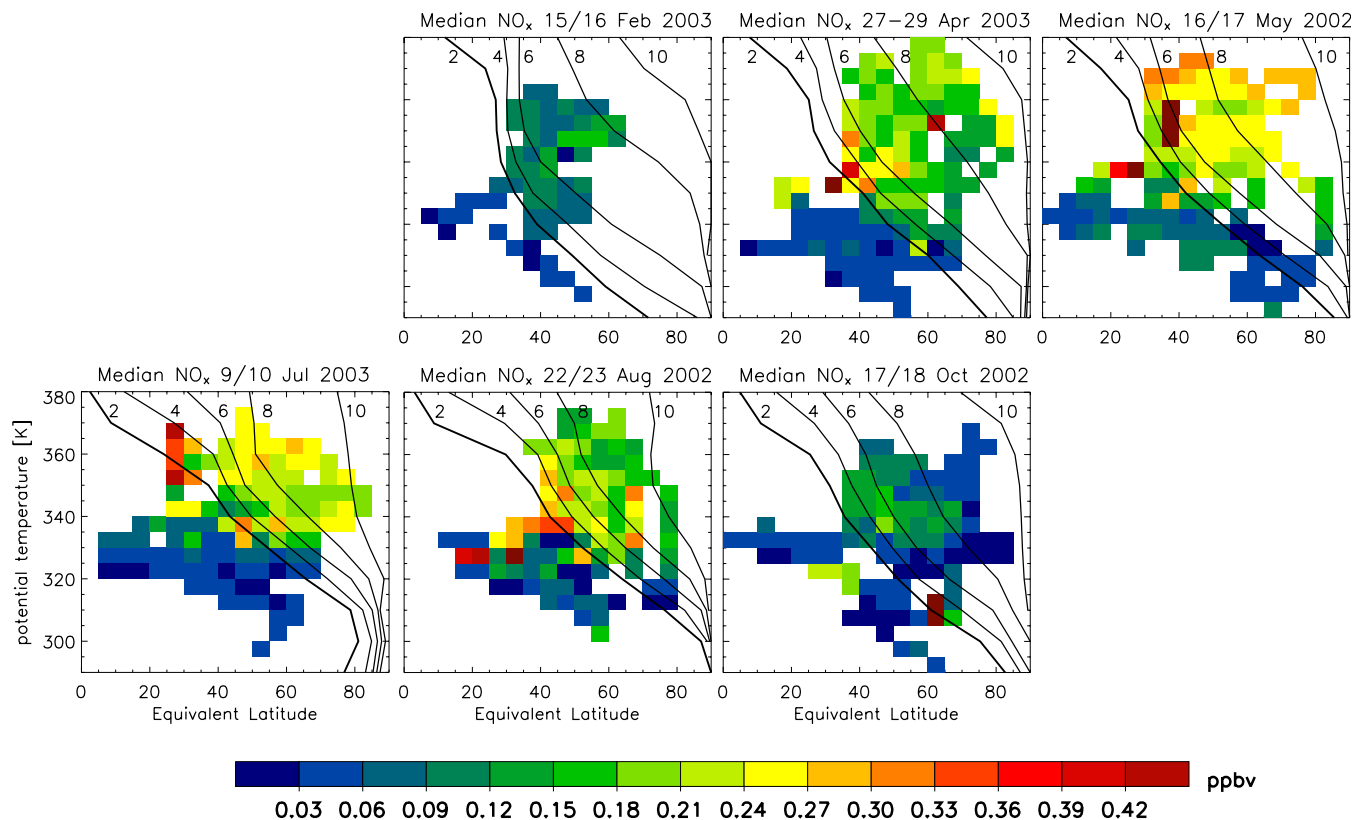
[1]Krebsbach, M., Günther, G., Spelten, N., and Schiller, C.: Characteristics of the extratropical transition layer as derived from H$_2$O and O$_3$ measurements in the UT/LS, Atmos. Chem. Phys. Discuss., to be submitted, 2006b.

**Fig. 5.** Same as Fig. 2, but for NO$_x$(=NO+NO$_2$).

4.2 Vertical tracer profiles

Vertical profiles in $\Delta\Theta$ relative to the tropopause of NO$_y$, N$_2$O, O$_3$, and NO$_x$ obtained for winter (DJF), spring (MAM), summer (JJA), and autumn (SON) are shown in Figs. 6 and 7. SPURT campaign data of two different years but corresponding to the same season are shown in the same vertical profile. In order to investigate a possible dependency of the vertical tracer distributions on latitude the data was classified and colored in the figures corresponding to its equivalent latitude into subtropical ($\phi_e < 35°$ N, blue), mid latitudinal (35° N $< \phi_e < 65°$ N, light grey), and polar air masses ($\phi_e > 65°$ N, green). Further, median tracer profiles have been calculated for each season (red lines).

Figures 6a and b show the vertical profiles of N$_2$O and NO$_y$ for each season. N$_2$O in general forms relatively compact profiles whereas NO$_y$ shows higher variability. The reason for this is that N$_2$O is almost uniformly distributed in the troposphere due to its low chemical reactivity and its low photodissociation cross-sections. Its only source is in the troposphere. NO$_y$, however, has additional sources in the UT/LMS beside its main stratospheric source as discussed above. Figure 7 shows the vertical profiles for O$_3$. Interestingly, the same qualitative features as found for NO$_y$ are also seen in the O$_3$ profiles. Upper tropospheric mixing ratios of

NO$_y$ and O$_3$ are higher in spring and summer than in autumn and winter by about 100% and 60%, respectively. The same seasonality for O$_3$ has been obtained by Krebsbach et al. (2006a) using 2-D probability distribution functions.

In the autumn panels of each figure, the vertical profiles of all seasons are shown together for comparison. The most obvious feature is a uniform distribution of the tracers in the troposphere and a strong gradient in the tracer mixing ratios beginning at around 5 K below the tropopause (with PV=2 PVU) as stated in the previous section. The gradients in the tracer profiles of NO$_y$, N$_2$O, and O$_3$ found across the tropopause (see Figs. 6a, b and 7a) are strongest in spring, decreasing throughout summer towards lowest gradients in autumn and increasing again during winter towards spring values. The gradients at the tropopause coincide with a strong gradient in static stability (cf. Pan et al., 2004). A tropopause based climatology of high-resolution radiosonde data by Birner et al. (2002) revealed that static stability exhibits a distinct maximum just above the extratropical tropopause, a feature not reproduced in ECMWF data which are used in the here presented study. However, the existence of the maximum in static stability and the coincident gradient in the tracer observations highlight the role of the tropopause to act as a transport barrier.
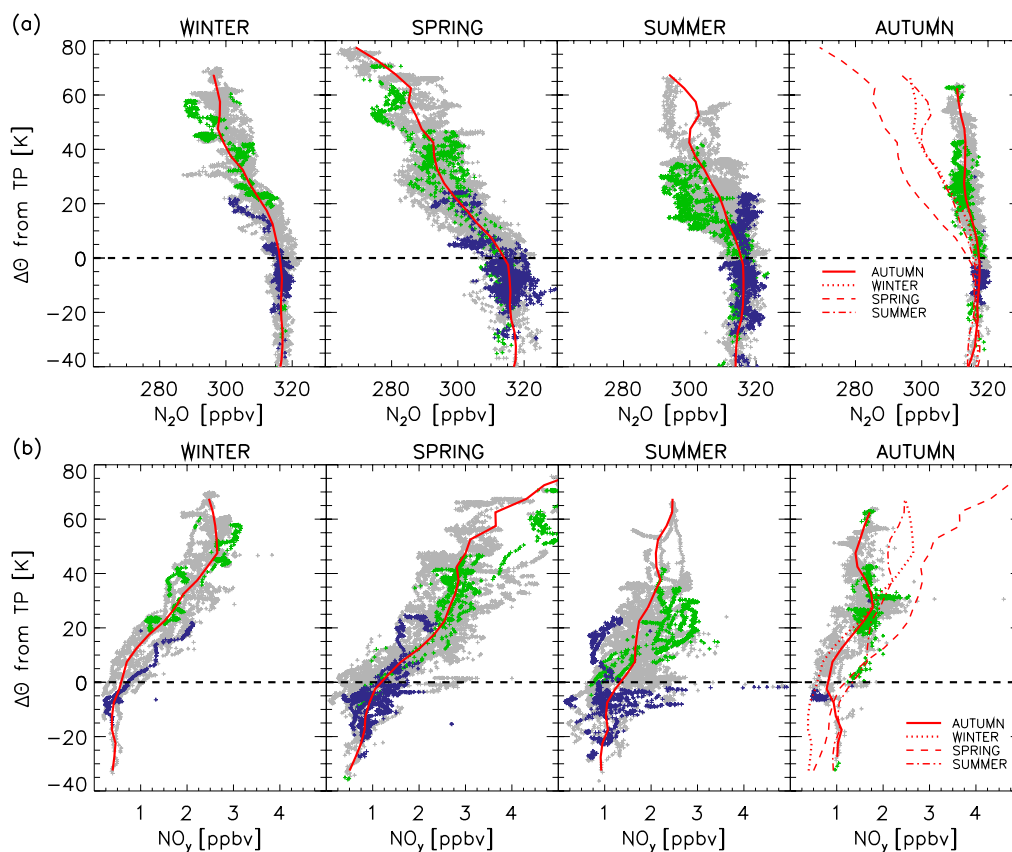
Fig. 6. Vertical profiles of **(a)** N$_2$O and **(b)** NO$_y$ mixing ratios as a function of $\Delta\Theta$ from the tropopause (defined by 2 PVU). Different panels show data for winter (DJF), spring (MAM), summer (JJA), and autumn (SON). Blue crosses denote measurements with ϕ_e south from 35° N, light grey crosses with ϕ_e between 35° N and 65° N, and green crosses with ϕ_e north from 65° N. Red lines denote profiles of median mixing ratios. In order to allow direct comparison, the winter, spring, and summer profiles are plotted in the autumn graph again.

The origin of the air masses is relevant since air from above 380 K is not purely aged stratospheric air but is rather a mixture containing also younger air from the tropical tropopause region (cf. Hoor et al., 2005). This topic will be investigated in the next section. Some of the tropospheric air transported into the LMS by troposphere-to-stratosphere transport (TST) might be removed later on by stratosphere-to-troposphere transport (STT). The effect of TST events further seems to be smoothed out by fast horizontal transport and mixing in the zonal direction as has been previously suggested by Hegglin et al. (2005). The result is a gradual transition from the troposphere into the stratosphere referred to as the extratropical tropopause transition layer. In summer the low gradient within this tropopause layer is therefore explained by both, a weaker Brewer-Dobson circulation and stronger tropospheric influence, filling up the LMS with tropospheric air as time proceeds towards autumn.

The vertical profiles of the shorter lived NO$_x$ for each season are shown in Fig. 7. In winter and autumn the vertical gradients in NO$_x$ together with the variability in NO$_x$ is relatively low. In spring and summer, however, a strong gradi-

ent exists across the tropopause and a bulge in the vertical profiles characterized by higher variability and higher NO$_x$ mixing ratios is obvious between 10 K below and 30 K above the tropopause. This feature is likely due to a combination of the increase in available sunlight enhancing NO$_x$ by photolysis of HNO$_3$, an increase in deep convection associated with lightning production of NO towards summer, and a weakening of the Brewer-Dobson circulation replacing less lowermost stratospheric air by STT. The low temperatures and low O$_3$ mixing ratios found in the tropopause region may further slow down chemical reaction rates of heterogeneous and gas-phase conversion of NO$_x$ into its reservoir species.

The classification of the air masses corresponding to their equivalent latitude (blue, light grey, green for subtropical, mid-latitudinal and polar data points) suggests that tracer profiles of NO$_y$, N$_2$O, and O$_3$ show no significant latitudinal dependency except in summer. The mixing ratios are mainly determined by their vertical distance relative to the tropopause and are similar for subtropical, mid latitude and polar air masses. In summer, however, mixing ratios of NO$_y$ and O$_3$ tend to be higher and lower for N$_2$O in the polar
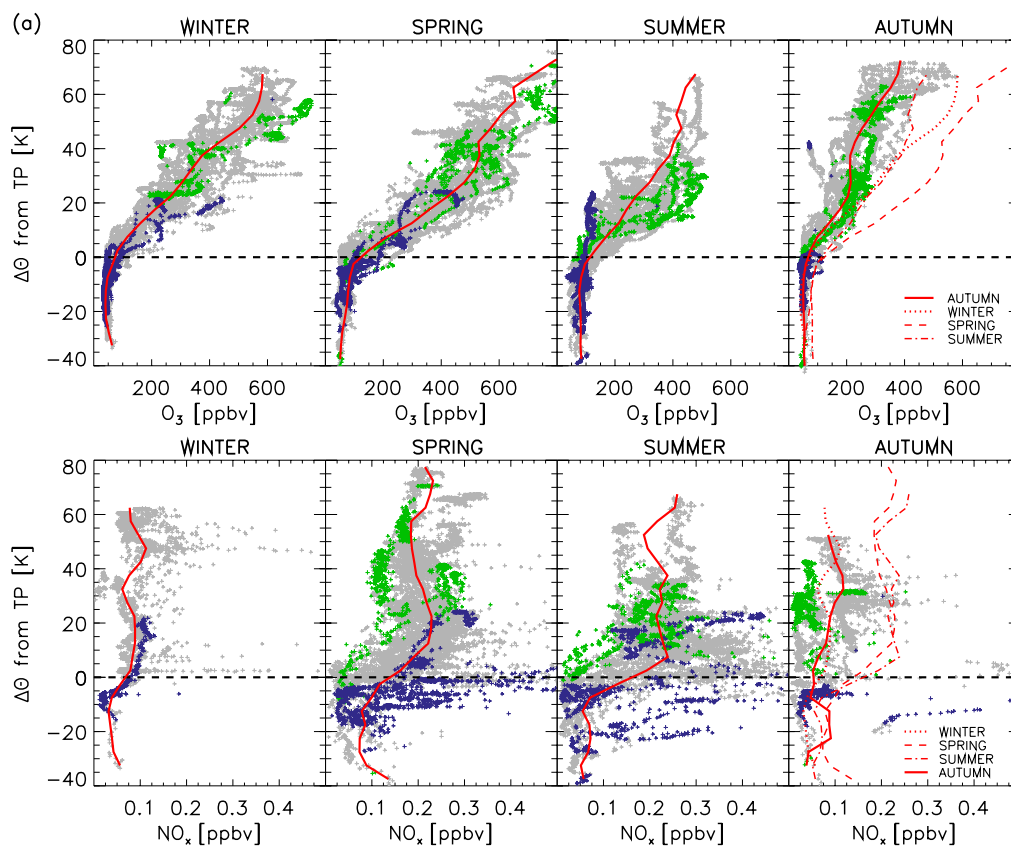
Fig. 7. Same as Fig. 6, but **(a)** for O$_3$ and **(b)** for NO$_x$ (=NO+NO$_2$).

region compared to values measured in the subtropics indicating a reservoir of older air at higher latitudes. It is interesting to see that the latitudinal gradient in potential vorticity is also most pronounced in summer with PV-isolines between 2 and 8 PVU lying closely together (see Fig. 2). This suggests that mixing and transport within the lowermost stratosphere which tend to smooth out latitudinal gradients are slower than time scales of processes which provide the lowermost stratosphere with tropospheric air starting in the beginning of summer and at lower latitudes. The latter may be associated with deep convective events which could also explain the highly variable NO$_x$ found in summer in the first 20 K above the tropopause. NO$_x$ also reveal a stronger dependency on ϕ_e than the other tracers during all seasons. Higher mixing ratios are found in regions south from 35° N, while lower values are found at higher ϕ_e.

In Fig. 8 finally, median NO$_x$ to NO$_y$ ratios are plotted as a function of altitude bins relative to the tropopause, for every season, and for subtropical, mid-latitudinal, and polar air masses according to the above classification. The number of data points per bin is indicated in the figure. Note, that the features in winter and autumn are less robust since NO was measured during one campaign only. The ratio of NO$_x$ to NO$_y$ presents an indicator for the chemical age of

an air mass. If the ratio is high, the air parcel may have experienced a recent input of NO$_x$, while low ratios indicate aged air masses in which the conversion of NO$_x$ into NO$_y$ already proceeded. Two main features in the NO$_x$ to NO$_y$ ratios should be highlighted in Fig. 8. Relatively low values in the "background" LMS above 20 to 30 K, and increasing ratios in descending towards the tropopause where a local maximum in the ratio exists. In winter, the profiles at mid-latitudes exhibit NO$_x$ to NO$_y$ ratios above 20 to 30 K with values around 0.025 [ppbv/ppbv]. Similar ratios are found in polar regions during spring and autumn. Comparable results have been found for the AASE II campaign during winter by Weinheimer et al. (1994). During spring, the "background" LMS ratios increase to values around 0.06 [ppbv/ppbv] and to values of around 0.08 [ppbv/ppbv] during summer, respectively. This difference can be explained by the seasonal cycle in available sunlight. More sunlight increases photolysis of HNO$_3$ leading to a production of NO$_2$ and hence increasing the NO$_x$ to NO$_y$ ratio while reaching photochemical equilibrium. With decreasing altitude, however, the NO$_x$ to NO$_y$ ratios and their variability increase. This feature is most pronounced in summer, but is also obvious in winter and spring. In winter, maximum values are around 0.1, in spring around 0.12, and in summer around 0.16 [ppbv/ppbv]. The existence
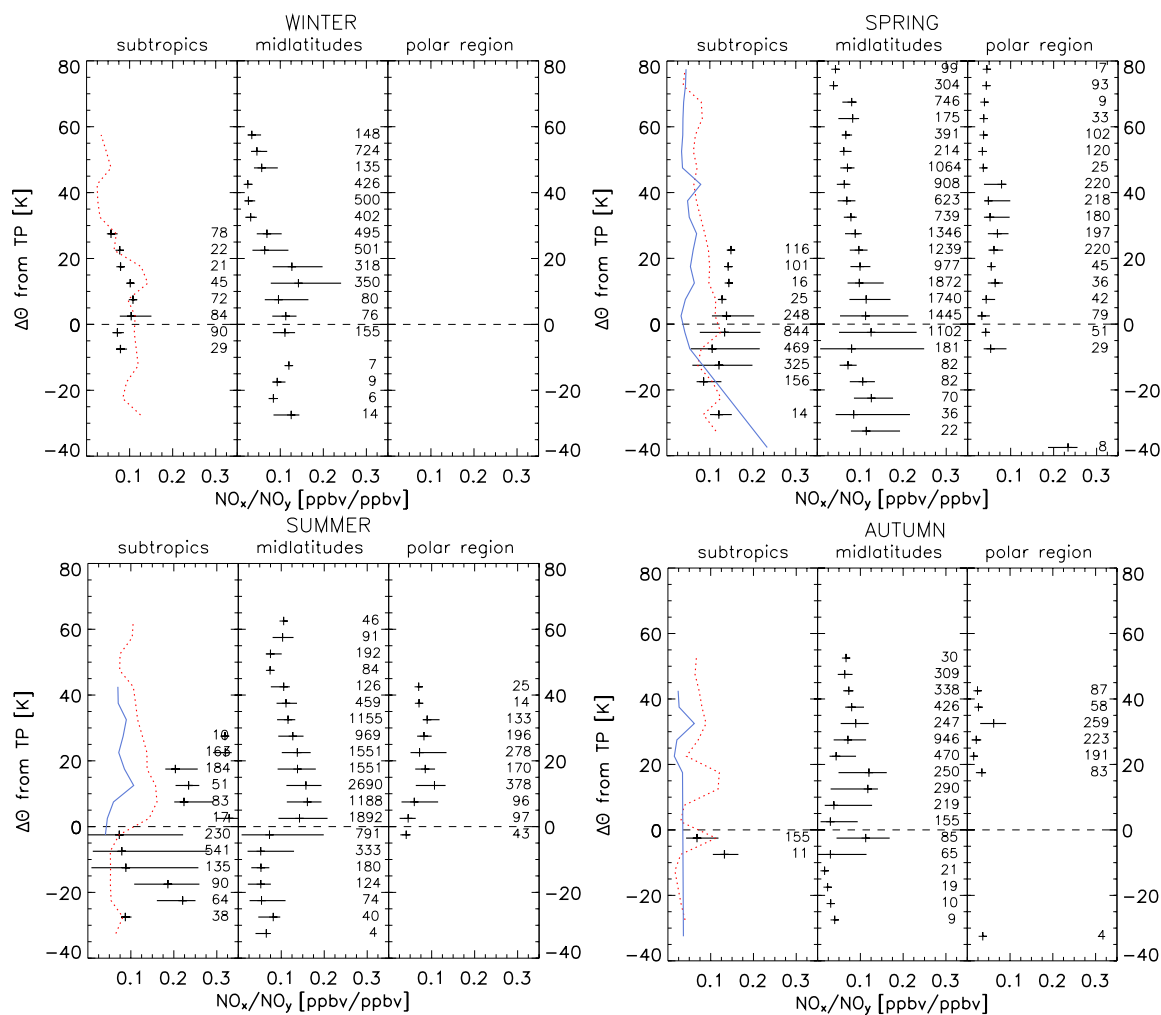
Fig. 8. Vertical profiles of median NO_x/NO_y ratios as a function of $\Delta\Theta$ from the tropopause (defined by 2 PVU) for each season. The data are classified by their equivalent latitude into subtropical ($\phi_e < 35°$ N), mid latitudinal ($35°$ N $< \phi_e > 65°$ N), and polar ($\phi_e > 65°$ N) air masses. Medians are calculated for bins of 5 K height. The number of measured data points per bin is indicated in the figure. Horizontal bars denote the range given by the mean NO_x/NO_y ratios $\pm$ the standard deviation. In order to allow direct comparison, the median profiles of the mid latitudes (red dotted line) and the polar region (blue line) are plotted in the subtropical class again.

of such maximum at the tropopause has been discussed in the literature previously (Weinheimer et al., 1994; Jaeglé et al., 1998; Ziereis et al., 2000). It was explained by a combination of the presence of NO_x sources and an enhanced lifetime of NO_x at the tropopause. Sources are likely to be deep convective injection of either polluted planetary boundary layer air or of air masses which were influenced by lightning (e.g. Hegglin et al., 2004). Aircraft emissions constitute another local source especially in the UT/LMS over Western Europe. The longer lifetime of NO_x in the tropopause region may be the result of slower reaction rates due to lower temperatures and lower O_3 values. These two factors slow down the conversion of NO_x to NO_y, whether by oxidation of NO_2 with OH, which leads to the formation of HNO_3, or by the heterogeneous conversion of N_2O_5 to HNO_3 after the

reaction between NO_2 and O_3. Except in winter, a strong latitudinal decrease in the NO_x to NO_y ratios is found with increasing latitude. This result might not only be linked to increased photolysis of HNO_3 at lower latitudes as stated by Weinheimer et al. (1994), but also to the source distribution of NO_x. In summer, we expect strongest convective activity associated with lightning in the subtropics (cf. Sect. 4.1). Highest variability of the NO_x to NO_y ratio found in the upper troposphere in the subtropics support this explanation.
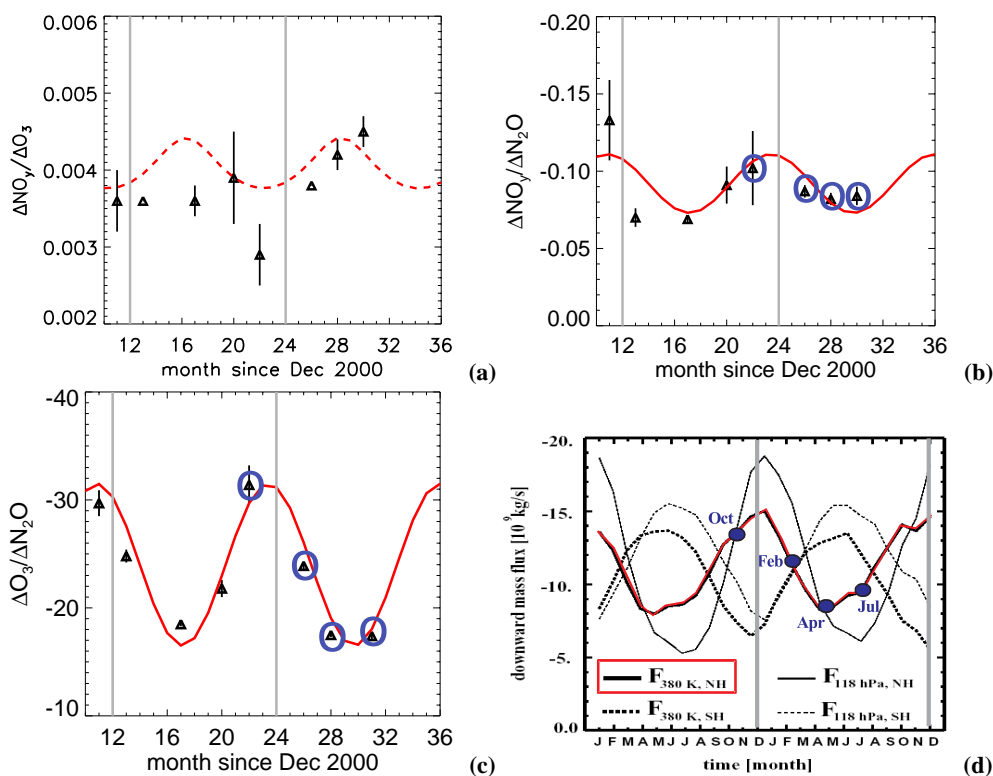
4.3 Seasonality of tracer-tracer correlations

Figure 9 shows correlation plots of O_3 with N_2O obtained during the different campaigns. For each data set, the correlation between O_3 and N_2O has been calculated by using stratospheric data points only with potential vorticity
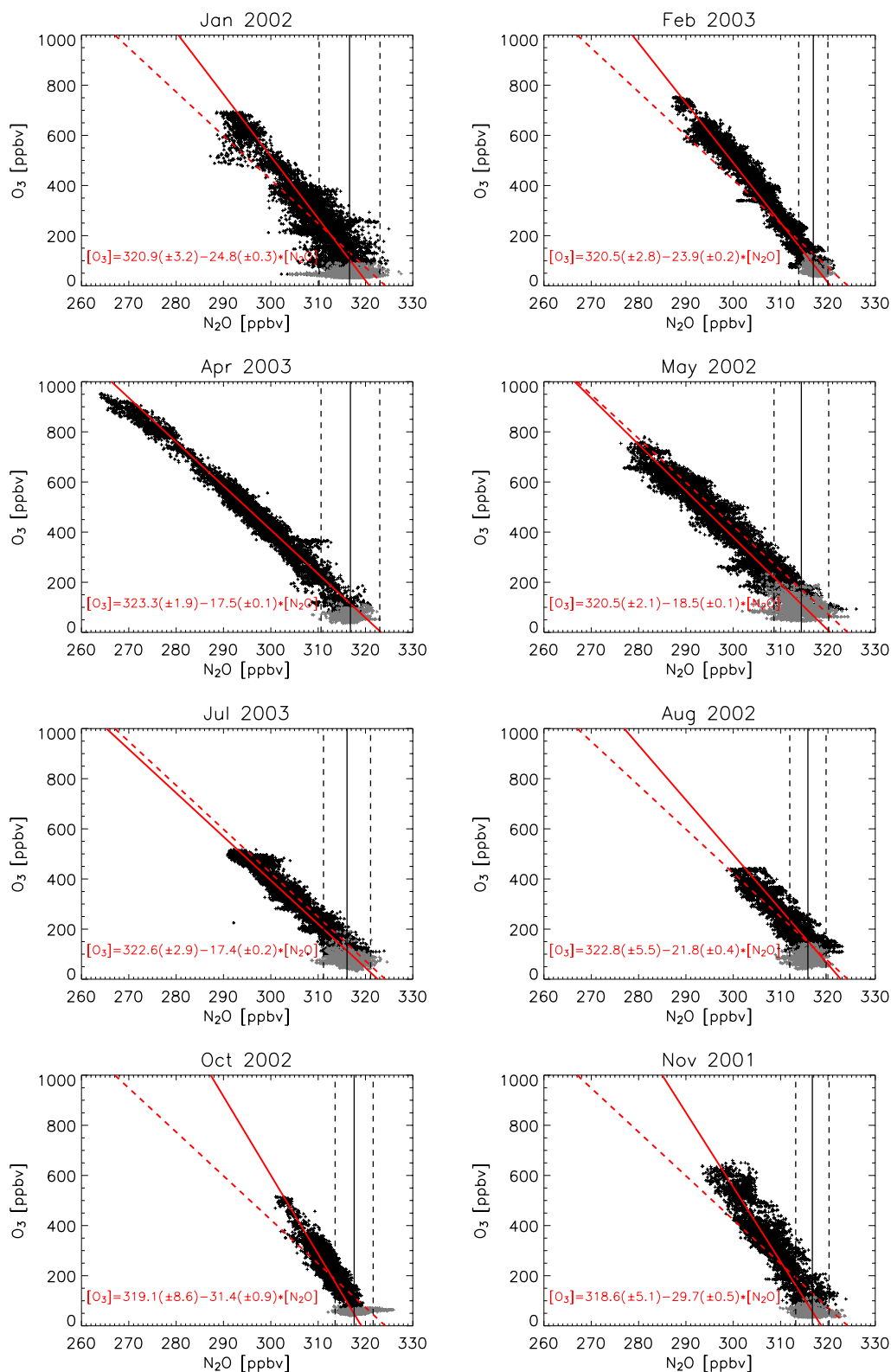
Fig. 9. Scatter plots between N$_2$O versus O$_3$ for each campaign. Grey data points indicate measurements in the troposphere (with PV<2). Red lines and formula specify linear fits to the stratospheric data considering errors in both tracers. In order to allow direct comparison the April fit is plotted in all panels (red dashed line). Black solid and dashed lines indicate the mean of tropospheric N$_2$O values ± their standard deviations (2σ).

Fig. 10. Slopes of tracer-tracer correlations measured during the SPURT campaigns in the "background" air of the LMS. **(a)** ΔNO$_y$/ΔO$_3$, **(b)** ΔNO$_y$/ΔN$_2$O, and **(c)** ΔO$_3$/ΔN$_2$O. The temporal evolution of the slopes exhibits a distinct seasonal cycle (given by the red lines) except for ΔNO$_y$/ΔO$_3$ (indicated by the red dashed line). **(d)** Downward mass fluxes through different reference surfaces adapted from Appenzeller et al. (1996). Reproduced by permission of American Geophysical Union. Here, the red line indicates the mass flux across the 380 K potential temperature surface being in phase with the seasonal cycle of the observed correlation slopes. Blue circles mark the months during which the last four SPURT campaigns were conducted.

>2 PVU. In general, the correlations between the two tracers are quite compact. They yield near-linear correlation coefficients (R^2) between 0.79 and 0.96. The compactness of the correlations indicate that the air masses in this region of the LMS are well mixed. Well mixed is used here for the mixing of air masses with different characters (e.g. air masses of tropical and mid-latitudinal origin) down to scales below the resolution of the observations. The compact correlation between the two tracers further may be a result of a combination of downward advection and strong horizontal mixing within the LMS similar to the theoretical framework for stratospheric tracer-tracer correlations provided by Plumb and Ko (1992). The only difference marks the effect of TST which is strongest for tracers with local sources such as NO$_y$. The correlations between NO$_y$ and N$_2$O therefore were calculated by only using data points with O$_3$ mixing ratios >300 ppbv in order to exclude air masses which show high variability in NO$_y$ due to tropospheric sources. The NO$_y$ and N$_2$O scatter plots are less compact (not shown). Correlation coefficients (R^2) for May 2002, February, April, and July 2003 campaigns are between 0.6 and 0.73, but smaller than 0.4 for the other campaigns. The more compact correlations found between February and July suggest that the LMS is domi-

nated during winter and spring by stratospheric air masses. On the other hand, the influence of the troposphere across the extratropical tropopause appears to become strongest between August and November, leading to less compact correlations between NO$_y$ and N$_2$O (see Hegglin, 2004).

For both tracer-tracer combinations, the correlations obtained in different years but corresponding to the same season show similar average slopes (ΔO$_3$/ΔN$_2$O and ΔNO$_y$/ΔN$_2$O). In Figs. 10b and c, the obtained correlation slopes are plotted as a function of time. The SPURT data set suggests, that the correlation slopes follow a seasonal cycle indicated by the red lines. The slopes of the NO$_y$ to N$_2$O correlation show changes by 20% between October 2002 (slope $=-0.102$) and April 2003 (slope $=-0.082$). This result is significantly higher than the maximum change in slope of 6% derived from ER2-data above 400 K during the ASHOE/MAESA and the STRAT campaigns (Keim et al., 1997). Their observed slopes were –0.069 in April 1994 and –0.073 in January 1996. The difference of the two observations may be explained by the different altitude range of the observations or the inter-annual variability in the strength of the mean meridional circulation.
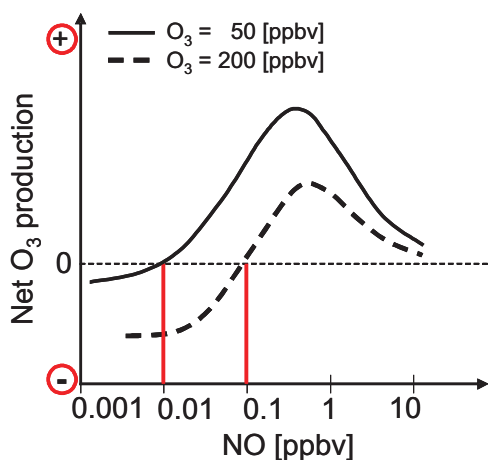
Fig. 11. Theoretical scheme of the net O$_3$ production as function of NO (thick black lines). As shown in chemical box model calculations by Grooss et al. (1998), critical NO values (marked by the red lines) depend on background O$_3$ mixing ratios . Thin black dashed line indicates zero O$_3$ production.

The observed seasonal cycle in the correlation slopes is roughly in phase with the downward mass flux calculated by Appenzeller et al. (1996) shown in Fig. 10d. The largest mass fluxes across a reference surface (e.g. the 380 K isentrope) coincide with the steepest correlation slopes, while smaller mass fluxes found in spring are coincident with more shallow slopes. The largest fraction of aged stratospheric air in the LMS is therefore found at the end of a period with strongest downward mass transport.

The changing slopes also indicate changing air mass origin. It suggests that the influence of the Brewer Dobson circulation on the measured slopes is superimposed by the rate at which tropical air is transported to mid-latitudes. This region lies between the tropical tropopause and around 420 K and is referred to as the tropically controlled transition region (Rosenlof et al., 1997). In order to explain the connection of this fast transport with the changing slope values we have to consider the mean distributions of correlation slopes. Fahey et al. (1990) presented the distribution of $\Delta NO_y/\Delta N_2O$ ratios in the lower stratosphere calculated by a 2-D chemical transport model. They showed that high absolute values are found in the tropical lower stratosphere, whereas low absolute values are found at higher altitudes and latitudes. Bregman et al. (2000) further analyzed the $\Delta O_3/\Delta N_2O$ ratios within the lower stratosphere obtained by a 3-D chemical transport model and found a latitudinal dependency with decreasing absolute values towards higher latitudes. They both explained their findings by the combined effects of transport and the photochemical aging of air masses.

Small absolute values of both, $\Delta O_3/\Delta N_2O$, and $\Delta NO_y/\Delta N_2O$, as found during spring in our study suggest therefore the presence of a large fraction of aged air masses originating from higher altitudes and latitudes. They either

are chemically processed on their way to higher latitudes and during descent in the polar vortex, or influenced by air descending from altitudes above 35–40 km where the linear relationships between the discussed tracers reverses sign. On the other hand, large absolute values of the correlation slopes as found during autumn represent younger air masses typical for the tropical lower stratosphere region and which took a "shorter" pathway leading more directly from the tropical tropopause to the LMS region. Winter and summer represent intermediate stages. Our findings are in close agreement with Hoor et al. (2005) who showed that the contribution of tropical tropospheric air (originating from above 370 K) to the chemical composition of the LMS amounts to about 35% in spring, while in autumn the contribution is about 55%.

It is interesting to note, that the slopes of the NO$_y$ to O$_3$ correlation slopes show no clear seasonal cycle (see Fig. 10a). The only significantly lower value in the slope was found during October 2002. Murphy et al. (1993) showed a latitudinal increase in the NO$_y$ to O$_3$ ratios from 0.002 to around 0.004 by going from the tropics to higher latitudes. This supports the finding that the air in October took a more direct way from the tropics to the LMS.

The SPURT data presented here do not resolve the question whether the observed slopes during spring and summer are the result of mixing with air masses which experienced enhanced chemical ozone loss and denitrification or whether they result from transport and mixing processes with air above the O$_3$ and NO$_y$ maxima where different correlation-characteristics prevail (Michelsen et al., 1998; Plumb et al., 2000; Proffitt et al., 2003). For this purpose other tracer-tracer correlations e.g. between CH$_4$ and N$_2$O can be used, which are not influenced by chemical processes. Since the dynamical range of the SPURT CH$_4$ data was not large enough to obtain compact correlations we were not able to look into this in more detail. Nevertheless, the vertical profiles of the CH$_4$ mixing ratios (not shown) also exhibit a seasonal cycle similar to what has been seen in Figs. 6a, b, and Fig. 7a, suggesting that rather the origin of air than enhanced chemical processing influences the observed tracer distributions in the LMS.

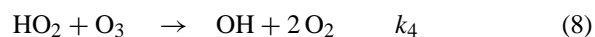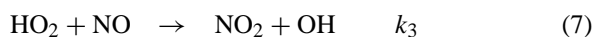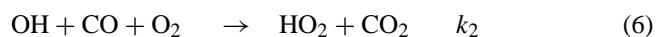### 4.4 Chemical regime: ozone destruction or production

The chemical composition and the physical characteristics of the UT/LMS, together with the influence of complex dynamical processes on small and large scales, make this region difficult to simulate in global chemical transport models (Brunner et al., 2003). In particular, large differences between modeled and measured NO$_x$ call for a more accurate description of NO$_x$ sources. The coverage of the UT/LMS with highly resolved tracer measurements obtained during SPURT, including the key species for ozone chemistry (NO and CO), can be used to determine the height at which the chemical regime switches from O$_3$ production to O$_3$ destruction.
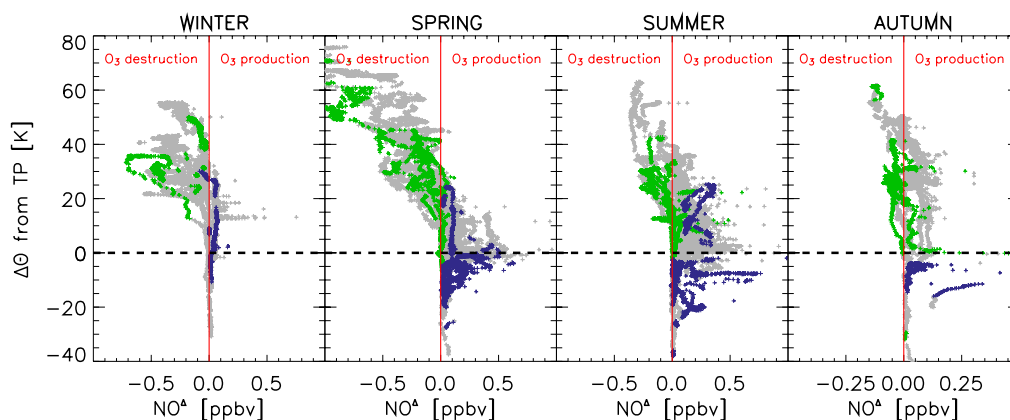
Fig. 12. Vertical profiles of excess NO (NO$^\Delta$) calculated for each measurement point as a function of $\Delta\Theta$ from the tropopause (defined by 2 PVU). Different panels show different seasons. Blue crosses denote measurements with ϕ_e south from 35° N, light grey crosses with ϕ_e between 35° N and 65° N, and green crosses with ϕ_e north from 65° N.

Figure 11 shows schematically the dependence of net O$_3$ production on available NO and on background O$_3$ mixing ratios as well as the NO$_{crit}$ values at which O$_3$ destruction turns into O$_3$ production (indicated by the red lines). It is based on the results by Grooss et al. (1998), using the Mainz two-dimensional photochemical model for upper tropospheric conditions assuming CO and HNO$_3$ mixing ratios of 60 ppbv and 0.2 ppbv, respectively. They showed that the NO$_{crit}$ value increases with increasing O$_3$ mixing ratios from values around 0.01 ppbv at 50 ppbv O$_3$ to 0.1 ppbv at 200 ppbv O$_3$. They showed that decreases in the CO mixing ratio decrease peak net O$_3$ production, but have no influence on NO$_{crit}$. Grooss et al. (1998) further showed that the NO+HO$_2$ reaction dominates O$_3$ production. Volatile organic compounds may therefore be neglected in a first approximation. It is clear from Fig. 11 that net O$_3$ production is highly nonlinear below and above the critical NO mixing ratio. O$_3$ production is further maximized at some NO value larger than NO$_{crit}$. Above this NO value, additional NO reduces O$_3$ production. It is therefore important to know the amount by which NO exceeds NO$_{crit}$ in order to know which chemical regime prevails. This is especially important when attempting to assess the chemical impact of additional, highly localized, NO$_x$ sources such as aircraft emissions and lightning on UT/LMS O$_3$ chemistry, and its feedback on climate.

In calculating the critical NO mixing ratios (NO$_{crit}$) at which net O$_3$ production changes from negative to positive, we assume the following chemistry to be important:

$$OH + O_3 \rightarrow HO_2 + O_2 \quad k_1 \quad (5)$$
$$OH + CO + O_2 \rightarrow HO_2 + CO_2 \quad k_2 \quad (6)$$
$$HO_2 + NO \rightarrow NO_2 + OH \quad k_3 \quad (7)$$
$$HO_2 + O_3 \rightarrow OH + 2O_2 \quad k_4 \quad (8)$$
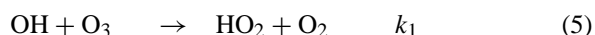
with k_1 to k_4 being pressure or temperature dependent reaction rates according to JPL/NASA (2003). The temporal change in O$_3$ then is given by

$$\frac{d[O_3]}{dt} = -k_1[OH][O_3] - k_4[HO_2][O_3] + k_3[HO_2][NO] \quad (9)$$

and the temporal change in OH by

$$\frac{d[OH]}{dt} = -k_1[OH][O_3] - k_2[OH][CO]$$
$$+ k_3[HO_2][NO] + k_4[HO_2][O_3]. \quad (10)$$

Imposing steady state onto both Eqs. (9) and (10) yields the following expression for a critical NO value valid in the UT/LMS region:

$$[NO_{crit}] = \frac{k_4}{k_3} \cdot [O_3] \cdot \left(1 + \frac{2k_1[O_3]}{k_2[CO]}\right). \quad (11)$$

In the troposphere where $2k_1O_3 \ll k_2CO$, NO$_{crit}$ approximates k_4O_3/k_3, the value derived by Crutzen (1979) for use in the troposphere. Above the tropopause, the temperature dependent reaction rate k_1 and O$_3$ increase, while the value in the denominator decreases due to decreasing CO mixing ratios and a pressure dependent reaction rate k_2. The term in brackets therefore gains in importance and changes NO$_{crit}$ significantly. In this approximation of NO$_{crit}$, we do not account for effects of halogen compounds such as Br or Cl, which might be important in both the upper troposphere and the lower stratosphere (von Glasow et al., 2004; Salawitch et al., 2005). However, if measured NO exceeds the calculated critical NO-mixing ratio chemical conditions favor O$_3$ production. If measured NO is lower than NO$_{crit}$, O$_3$ destruction is expected. NO$_{crit}$ is calculated for each sampled air mass using the SPURT CO (Hoor et al., 2004), O$_3$, temperature and pressure data. We define excess NO (NO$^\Delta$) as

a measure of how much NO is available in addition to NO$_{crit}$ in each air mass according to:

$$NO^\Delta = NO_{meas} - NO_{crit} \qquad (12)$$

where NO$_{meas}$ are the measured NO mixing ratios.

Figure 12 shows the NO$^\Delta$ values during the SPURT measurements in $\Delta\Theta$ relative to the tropopause for each season. In winter, the NO$^\Delta$ values in the upper troposphere and lowermost stratosphere up to a height of 15 K above the tropopause are close to zero. Any source of NO at these altitudes will likely lead to O$_3$ production. Above 15 K relative to the tropopause, however, the chemical regime switches to O$_3$ destruction. In spring and summer, the picture changes significantly. NO$^\Delta$ values in the upper troposphere and lowermost stratosphere up to 20 K and 30 K above the tropopause, respectively, are strongly positive. The NO$^\Delta$ values therefore imply significant O$_3$ production in this region. This finding is consistent with a study by Logan (1985) explaining increased O$_3$ values in the upper troposphere during spring and summer as a result of photochemical O$_3$ production. Above 20 K and 30 K for spring and summer, respectively, the chemical regime switches to O$_3$ destruction. NO$^\Delta$ is further more negative in spring than in summer. In autumn finally, NO$^\Delta$ values are very low (note the different scale for the x-axis in Fig. 12). Nevertheless, they suggest, that the LMS at mid-latitudes favors O$_3$ production for $\Delta\Theta$ values up to 40 K above the tropopause. Additional NO up to this height may therefore have a high potential for O$_3$ production. The vertical profiles in the polar regions further turn in general at lower altitudes into the O$_3$ destruction regime. In Fig. 13 finally, we calculated mean vertical profiles of NO$_{crit}$ relative to the tropopause. The NO$_{crit}$ values show a seasonal cycle with highest values in spring and lowest in autumn. This reflects its dependence on the background O$_3$ mixing ratios which also show a maximum in spring and a minimum during autumn. A significant amount of CO in the LMS decreases NO$_{crit}$ values according to Eq. (11). Less NO is therefore necessary to turn the region into the O$_3$ production regime. This is the case during autumn, when tropospheric influence on the LMS is highest as derived from CO measurements (Hoor et al., 2005).

The chemical regime in the UT/LMS is according to this study is strongly dependent on altitude relative to the tropopause and on season. Both factors determine the fraction of tropospheric air and the background O$_3$ mixing ratios in the LMS. Koch et al. (2002) found positive O$_3$ trends in the UT/LMS region depending on season and reaching maximum altitudes in autumn. Chemical production may therefore serve as an explanation for these trends assuming a positive trend would also exist in available NO. While the next step should be the quantification of net O$_3$ production by using a more complex chemistry model including all important reactions in the tropopause region, the results presented here may be useful to validate the chemical regimes obtained in global chemistry transport models.

5 Conclusions

A new measuring system for high resolution and high sensitivity measurements of NO$_y$, NO, and O$_3$ was implemented into a Learjet 35A aircraft. The measurements were performed simultaneously using a three-channel chemiluminescence detector and an externally mounted converter in which NO$_y$ species were reduced catalytically to NO on a heated gold surface in the presence of CO. The semi-automated system was successfully operated during a total of six measurement campaigns plus two campaigns with an older system performed seasonally between November 2001 and July 2003 in the framework of the SPURT project. The mission flights covered the UT/LMS region over Europe from 30° to 75° N up to a potential temperature of 380 K.

When presented in the equivalent latitude–potential temperature framework, the SPURT distributions of NO$_y$, N$_2$O, and O$_3$ in the LMS are quite simple. There is a gradual increase in mixing ratio with increasing distance from the tropopause, and a strong seasonal variation. During winter and spring, NO$_y$ and O$_3$ mixing ratios are high, whereas N$_2$O mixing ratios are low. During summer and autumn, N$_2$O mixing ratios are close to tropospheric values, while O$_3$ and NO$_y$ mixing ratios are low. These changes show that the seasonal cycle of the Brewer-Dobson circulation has a dominating influence on tracer distributions in the LMS. There are strong gradients near the tropopause, both in the vertical across isentropes, and in the horizontal along isentropes. Our measurements therefore show that the extratropical tropopause acts as a barrier to transport and mixing in both vertical and horizontal directions. Vertical transport through the tropopause is inhibited by a strong gradient in static stability (cf. Birner, 2002; Pan et al., 2004), whereas quasi-horizontal transport along isentropes near the tropopause is inhibited by a strong meridional PV gradient (cf. Birner, 2006). The abundance of NO$_x$ is dependent on the available sunlight, and therefore shows enhanced values in spring and summer. Higher variability in NO$_x$ is found around the subtropical jet.
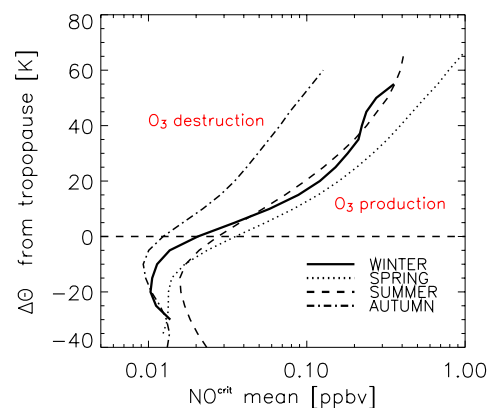
Vertical profiles in $\Delta\Theta$ relative to the tropopause show compact distributions of O$_3$, N$_2$O, and NO$_y$. The different tracers exhibit strong vertical gradients across the tropopause. The gradients are strongest in spring, intermediate in winter and summer, and weakest in autumn. Except in summer, there are no latitudinal gradients in the LMS. This supports the view that there are no additional transport barriers within the LMS, and that the LMS can be interpreted as a dynamically well-mixed layer, as reported by Birner (2006). The latitudinal tracer gradient during summer may arise from a stronger meridional PV gradient, from a decrease in dynamical activity which results in less meridional mixing, and ultimately from enhanced transport of tropospheric air into the LMS by various TST events starting at lower latitudes. NO$_x$ shows higher values in spring and summer compared to autumn and winter. Interestingly, it exhibits

a local maximum within the first 20 K above the tropopause. Simultaneously, a maximum is seen in the vertical profiles of the NO$_x$/NO$_y$ ratio. It indicates an accumulation of NO$_x$ from sources like aircraft emissions, deep convective injection of polluted planetary boundary layer air, or lightning. If this feature persists in evaluations of larger data sets, it might have strong implications for net O$_3$ production in this region.

Scatter plots of O$_3$ against N$_2$O, and of NO$_y$ against N$_2$O, obtained during SPURT show compact correlations. This implies that the concept of tracer-tracer correlations may also be used within the LMS. There is, however, one restriction. In the case of NO$_y$ and N$_2$O, data points which lie below 300 ppbv O$_3$ should not be used. Below this ozone mixing ratio, NO$_y$ can be highly perturbed by TST, a process which can significantly alter the calculated correlation slopes. However, for tracers which are well-mixed in the troposphere, the compactness of the correlations is less influenced by TST.

The correlations between O$_3$ and N$_2$O, as well as between NO$_y$ and N$_2$O, reveal pronounced seasonal cycles which are in phase with the calculated mass fluxes across the 380 K isentrope derived by Appenzeller et al. (1996). The diabatically descending air originates from the tropically controlled transition region (Rosenlof et al., 1997). Its composition depends on the strength of the Brewer Dobson circulation and the rate of transport and mixing between the tropics and the mid-latitudes. The values of the seasonally changing slope therefore offer insight into the origin of air masses in the LMS. The shallow slopes of ΔNO$_y$/ΔN$_2$O and ΔO$_3$/ΔN$_2$O in spring indicate the presence of a large fraction of aged stratospheric air, i.e. air which traveled through high altitudes and/or high latitudes and probably descended in the polar vortex. On the other hand, steeper slopes in autumn indicate the presence of young air which may have taken a "shorter" pathway leading from the tropical tropopause region to the LMS. The slope of the correlation between NO$_y$ and O$_3$ exhibits no pronounced seasonal cycle, but the lower values found in autumn also support the presence of tropical air masses (cf. Murphy et al., 1993). Our findings are qualitatively in agreement with the findings by Hoor et al. (2005) who showed that the contribution of tropical tropospheric air to the chemical composition of the LMS amounts to about 35% in spring, while in autumn the contribution is about 55%. The strong horizontal gradients found in the tracer distributions at the tropopause and a pronounced phase shift of two months between tropospheric and lowermost stratospheric CO$_2$ mixing ratios suggest that the air with tropospheric character found in the "background" LMS originates from the tropical tropopause region above around 370 K (Hoor et al., 2004). While quasi-isentropic transport below 380 K has been shown to significantly contribute to the LMS tracer composition at flight locations of 34.5°N in September (Ray et al., 1999), our findings imply that this transport pathway has less impact on the "background" LMS tracer composition at latitudes between 40° N and 70° N.

The seasonal cycle in the correlation slopes in the LMS

Fig. 13. Vertical profiles of mean critical NO (NO$_{crit}$) in $\Delta\Theta$ relative to the tropopause (defined by 2 PVU). Different linestyles indicate different seasons.

is likely to be influenced by the inter-annual variability in the strength of the Brewer-Dobson circulation and in the rate at which air is transported from the tropics to mid-latitudes. Tracer-tracer correlations therefore may be used in future as a valuable measure of the circulation strength. They may also serve as indicators for changing air mass origin or photochemical aging. Finally, the seasonal variability of the NO$_y$ to N$_2$O ratio must be taken into account when calculating excess NO$_y$ which is commonly used as a measure for sources and sinks of NO$_y$ in the stratosphere.

The seasonal change in the composition of the UT/LMS (i.e. the seasonal change in background O$_3$ mixing ratios and the influence of the tropospheric trace gas species NO$_x$ and CO) has an important effect on chemistry in this region. The SPURT NO measurements provide highly resolved measurements of key species involved in O$_3$ chemistry. In this study, the critical NO values (NO$_{crit}$) at which net O$_3$ production changes from positive to negative were calculated in a way which accounted for both the tropospheric and the stratospheric character of air in the LMS. We also calculated the excess NO value (NO$^\Delta$), a measure of the amount of NO which exceeds NO$_{crit}$. The results show that during spring and summer, O$_3$ production occurs throughout the upper troposphere, and in the LMS up to heights of 20 and 30 K above the local tropopause, respectively. Above these heights, and especially in winter, the composition of the LMS leads to O$_3$ destruction. In autumn, NO$^\Delta$ is slightly above zero up to heights of 40 K above the local tropopause. Here, additional sources of NO will lead to enhanced O$_3$ production. The SPURT data set is a valuable contribution toward a global climatology of NO$_y$, N$_2$O, NO, and O$_3$, among other long-lived species. Through the specific campaign setup, the measurements provide both representative information on long-lived tracer distributions, as well as insight into individual processes shaping the chemical structure of the tropopause region (cf. Hegglin et al., 2004). The dataset is therefore an

ideal platform from which different issues concerning transport and mixing processes in the tropopause region can be addressed. In particular, it might be useful for validation of satellite measurements or of transport and mixing processes within the UT/LMS in global chemistry transport models. However, the conclusions drawn in this paper apply strictly only to the UT/LMS in the longitude sector from –20° E to 30° E in the Northern hemisphere. Finally, to confirm the presented conclusions, further investigations should be made by using model simulations and applying the presented evaluation methods to larger data sets. More measurements, preferentially over an even broader range of ϕ_e and Θ are needed to better characterize the latitudinal gradients of the presented tracers. Future aircraft observations should be conducted at different longitudes and extended into the southern hemisphere in order to enhance global knowledge of tracer distributions in the UT/LMS.

Edited by: P. Haynes

References

Appenzeller, C., Holton, J. R., and Rosenlof, K. H.: Seasonal variation of mass transport across the tropopause, J. Geophys. Res., 101, 15 071–15 078, 1996.

Baehr, J., Schlager, H., Ziereis, H., Stock, P., van Velthoven, P., Busen, R., Ström, J., and Schumann, U.: Aircraft observations of NO, NO$_y$, CO, and O$_3$ in the upper troposphere from 60° N to 60° S – Interhemispheric differences at midlatitudes, Geophys. Res. Lett., 30(11), 1598, doi:10.1029/2003GL016935, 2003.

Birner, T.: Fine-scale structure of the extratropical tropopause region, J. Geophys. Res., 111, D04104, doi:10.1029/2005JD006301, 2006.

Birner, T., Dörnbrack, A., and Schumann, U.: How sharp is the tropopause at midlatitudes?, Geophys. Res. Lett., 29, 45-1, doi:10.1029/2002GL015142, 2002.

Bregman, B., Lelieveld, J., van de Broek, M., Siegmund, P., Fischer, H., and Bujok, O.: N$_2$O and O$_3$ relationship in the lowermost stratosphere: A diagnostic for mixing processes as represented by a three-dimensional chemistry-transport model, J. Geophys. Res., 105, 17 279–17 290, 2000.

Brunner, D., Staehelin, J., Jeker, D., Wernli, H., and Schumann, U.: Nitrogen oxides and ozone in the tropopause region of the Northern Hemisphere: Measurements from commercial aircraft in 1995/96 and 1997, J. Geophys. Res., 106, 27 673–27 699, 2001.

Brunner, D., Staehelin, J., Rogers, H. L., et al.: An evaluation of the performance of chemistry transport models by comparison with research aircraft observations. Part 1: Concepts and overall model performance, Atmos. Chem. Phys., 3, 1609–1631, 2003.

Butchart, N. and Remsberg, E. E.: The area of the stratospheric polar vortex as a diagnostic tracer for transport on an isentropic surface, J. Atmos. Sci., 45, 1319–1339, 1986.

Crawford, J., Davis, D., Chen, G., et al.: Photostationary state analysis of the NO$_2$-NO system based on airborne observations from the western and central north pacific, J. Geophys. Res., 101, 2053–2072, 1996.

Crutzen, P.: The role of NO and NO$_2$ in the chemistry of the troposphere and the stratosphere, Ann. Rev. Earth Planet. Sci., 7, 443–472, 1979.

Emmons, L. K., Hauglustaine, D. A., Müller, J.-F., Carrol, M. A., Brasseur, G. P., Brunner, D., Staehelin, J., Thourit, V., and Marenco, A.: Data composites of airborne observations of tropospheric ozone and its precursors, J. Geophys. Res., 105, 20 497–20 538, 2000.

Engel, A., Bönisch, H., Brunner, D., et al.: Highly resolved observations of trace gases in the lowermost stratosphere and upper troposphere from the Spurt project: an overview, Atmos. Chem. Phys., 6, 283–301, 2006.

Fahey, D. W., Eubank, C. S., Hubler, G., and Fehsenfeld, F. C.: Evaluation of a catalytic reduction technique for the measurement of total reactive odd-nitrogen NO$_y$ in the atmosphere, J. Atmos. Chem., 3, 435–468, 1985.

Fahey, D., Solomon, S., Kawa, S., Loewenstein, M., Podolske, J., Strahan, S., and Chan, K.: A diagnostic for denitrification in the winter polar stratosphere, Nature, 345, 698–702, 1990.

Fontijn, A., Sabadell, A., and Ronco, R.: Homogenous chemiluminescent measurement of nitric oxide with ozone, Angewandte Chemie, 42, 575–579, 1970.

Forster, P. and Shine, K.: Radiative forcing and temperature trends from stratospheric ozone changes, J. Geophys. Res., 105, 10 169–10 857, 1997.

Garcia, R., Stordal, F., Solomon, S., and Kiehl, J.: A new numerical model of the middle atmosphere, 1. Dynamics and transport of tropospheric source gases, J. Geophys. Res., 97, 12 967–12 991, 1992.

Grooss, J. U., Brühl, C., and Peter, T.: Impact of aircraft emissions on tropospheric and stratospheric ozone. Part I: Chemistry and 2-D model results, Atmos. Environ., 32, 3173–3184, 1998.

Hegglin, M. I., Brunner, D., Wernli, H., et al.: Tracing troposphere-to-stratosphere transport above a mid-latitude deep convective system, Atmos. Chem. Phys., 4, 741–756, 2004.

Hegglin, M. I.: Airborne NO$_y$-, NO- and O$_3$-measurements during SPURT: Implications for atmospheric transport, Disseration, Eidgenössische Technische Hochschule ETH Zürich, Nr. 15553, http://e-collection.ethbib.ethz.ch/show?type=diss&nr=15553, 2004.

Hegglin, M. I., Brunner, D., Peter, T., Staehelin, J., Wirth, V., Hoor, P., and Fischer, H.: Determination of eddy-diffusivity in the lowermost stratosphere, Geophys. Res. Lett., 32, L13812, doi:10.1029/2005GL022495, 2005.

Holton, J., Haynes, P., McIntyre, M., Douglass, A., Rood, R., and Pfister, L.: Stratosphere-troposphere exchange, Rev. Geophys., 33, 403–439, 1995.

Hoor, P., Fischer, H., Lange, L., and Lelieveld, J.: Seasonal vari-

ations of a mixing layer in the lowermost stratosphere as identified by the CO-O$_3$ correlation from in situ measurements, J. Geophys. Res., 107, D5–D6, 4044, doi:10.1029/2000JD000289, 2002.

Hoor, P., Gurk, C., Brunner, D., Hegglin, M. I., Wernli, H., and Fischer, H.: Seasonality and extent of extratropcial TST derived from in-situ CO measurements during SPURT, Atmos. Chem. Phys., 4, 1427–1442, 2004.

Hoor, P., Fischer, H., and Lelieveld, J.: Tropical and extratropical tropospheric air in the lowermost stratosphere over Europe: A CO-based budget, Geophys. Res. Lett., 32, L07802, doi:10.1029/2004GL022018, 2005.

IPCC (Intergovernmental Panel on Climate Change): Aviation and the globale atmosphere, edited by: Penner, J. E., Lister, D. H., Griggs, D. J., Dokken, D. J., and McFarland, M., Cambridge University Press, New York, 29–64, 1999.

Jaeglé, L., Jacob, D. J., Wang, Y., Weinheimer, A. J., Ridley, B. A., Campos, T. L., Sachse, G. W., and Hagen, D. E.: Sources and chemistry of NO$_x$ in the upper troposphere over the United States, Geophys. Res. Lett., 25, 1705–1708, 1998.

James, P., Stohl, A., Forster, C., Eckhardt, S., Seibert, P., and Frank, A.: A 15-year climatology of stratosphere-troposphere exchange with a Lagrangian particle dispersion model, part B, Mean climate and seasonal variability, J. Geophys. Res., 108, D12, doi:10.1029/2002JD002639, 2003.

JPL/NASA: Chemical Kinetics and Photochemical Data for Use in Atmospheric Studies, JPL Publication 02-25, NASA Jet Propulsion Laboratory, California, 2003.

Keim, E., Loewenstein, M., Podolske, J., et al.: Measurements of the NO$_y$-N$_2$O correlation in the lower stratosphere: Latitudinal and seasonal changes and model comparisons, J. Geophys. Res., 102, 13 193–13 229, 1997.

Koch, G., Wernli, H., Staehelin, J., and Peter, T.: A Lagrangian analysis of stratospheric ozone variability and long-term trends above Payerne (Switzerland) during 1970–2001, J. Geophys. Res., 107, 4373, doi:10.1029/2001JD001550, 2002.

Kondo, Y., Koike, M., Kawakami, S., Singh, H. B., Nakajima, H., Gregory, G. L., Blake, D. R., Sachse, G. W., Merrill, J. T., and Newell, R. E.: Profiles and partitioning of reactive nitrogen over the Pacific Ocean in winter and early spring, J. Geophys. Res., 102, 28 405–28 424, 1997.

Krebsbach, M., Brunner, D., Günther, G., Hegglin, M., Maser, R., Mottaghy, D., Riese, M., Spelten, N., Wernli, H., and Schiller, C.: Seasonal cycles and variability of O$_3$ and H$_2$O in the UT/LMS during SPURT, Atmos. Chem. Phys., 6, 109–125, 2006a.

Lacis, A. A., Wuebbles, D. J., and Logan, J. A.: Radiative forcing of climate by changes in the vertical distribution of ozone, J. Geophys. Res., 95, 9971–9981, 1990.

Lange, L., Fischer, H., Parchatka, U., Gurk, C., Zenker, T., and Harris, G.: Characterization and application of an externally mounted catalytic converter for aircraft measurements of NO$_y$, Rev. Sci. Instrum., 73, 3051–3057, 2002.

Logan, J.: Tropospheric ozone: Seasonal behaviour, trends, and anthropogenic influence, J. Geophys. Res., 90, 10 463–10 482, 1985.

Michelsen, H. A., Manney, G. L., Gunson, M. R., and Zander, R.: Correlations of stratospheric abundances of NO$_y$, O$_3$, N$_2$O, and CH$_4$ derived from ATMOS measurements, J. Geophys. Res., 103, D21, 28 347–28 359, 1998.

Mottaghy, D.: Aufbau, Charakterisierung und Validierung eines in-situ Instrumentes zur Messung von Ozon in der oberen Troposphäre und unteren Stratosphäre, Diploma thesis, RWTH Aachen, 2001.

Murphy, D., Fahey, D., Proffitt, M., Liu, S., Chan, K., Eubank, C., Kawa, S., and Kelly, K.: Reactive nitrogen and its correlation with ozone in the lower stratosphere and upper troposphere, J. Geophys. Res., 98, 8751–8773, 1993.

Pan, L. L., Randel, W. J., Gary B. L., Mahoney, M. J., and Hintsa, E. J.: Definitions and sharpness of the extratropical tropopause: A trace gas perspective, J. Geophys. Res., 109, D23103, doi:10.1029/2004JD004982.

Pätz, H.-W., Volz-Thomas, A., Hegglin, M. I., Brunner, D., Fischer, H., and Schmidt, U.: In-situ comparison of the NO$_y$ instruments flown in MOZAIC and SPURT, Atmos. Chem. Phys. Discuss., 6, 649–671, 2006.

Plumb, R. A. and Ko, M.: Interrelationships between mixing ratios of long-lived stratospheric constituents, J. Geophys. Res., 97, 10 145–10 156, 1992.

Plumb, R. A., Waugh, D. W., and Chipperfield, M. P.: The effects of mixing on tracer relationships in the polar vortices, J. Geophys. Res., 105, D8, 10 047–10 062, 2000.

Proffitt, M. H., Aikin, K., Tuck, A. F., Margitan, J. J., Webster, C. R., Toon, G. C., and Elkins, J. W.: Seasonally averaged ozone and nitrous oxide in the Northern Hemisphere lower stratosphere, J. Geophys. Res., 108, D3, 4110, doi:10.1029/2002JD002657, 2003.

Ray, E. A., Moore, F. L., Elkins, J. W., Dutton, G. S., Fahey, D. W., Vömel, H., Oltmans, S. J., and Rosenlof, K. H.: Transport into the Northern Hemisphere lowermost stratosphere revealed by in situ tracer measurements, J. Geophys. Res., 104, 26 565–26 580, 1999.

Ridley, B. and Howlett, L.: An instrument for NO measurements in the stratosphere, Rev. Sci. Instrum., 45, 742–746, 1974.

Rosenlof, K. H., Tuck, A. F., Kelly, K. K., Russell, J. M., and Mc-Cornick, M. P.: Hemispheric asymmetries in water vapor and inferences about transport in the lower stratosphere, J. Geophys. Res., 102, 13 213–13 234, 1997.

Salawitch, R. J., Weisenstein, D. K., Kovalenko, L. J., Sioris, C. E., Wennberg, P. O., Chance, K., Ko, M. K. W., and McLinden, C. A.: Sensitivity of ozone to bromine in the lower stratosphere, Geophys. Res. Lett., 32, L05811, doi:10.1029/2004GL021504, 2005.

Sankey, D. and Shepherd, T. G.: Correlations of long-lived chemical species in a middle atmosphere general circulation model, J. Geophys. Res., 108, D16, 4494, doi:10.1029/2002JD002799, 2003.

Singh, H. B., Chen, Y., Gregory, G. L., Sachse, G. W., Talbot, R., Blake, D. R., Kondo, Y., Bradshaw, J. D., Heikes, B., and Thornton, D.: Trace chemical measurements from the northern midlatitude lowermost stratosphere in early spring: Distributions, correlations, and fate, Geophys. Res. Lett., 24, 127–130, 1997.

Sprenger, M. and Wernli, H.: A northern hemispheric climatology of cross-tropopause exchange for the ERA15 time period (1979–1993), J. Geophys. Res., 108, D12, 8521, doi:10.1029/2002JD002636, 2003.

Strahan, S., Loewenstein, M., and Podolske, J.: Climatology and samll-scale structure of lower stratospheric N$_2$O based on in situ observations, J. Geophys. Res., 104, 2195–2208, 1999a.

Strahan, S.: Climatologies of lower stratospheric NO$_y$ and O$_3$ and correlations with N$_2$O-based on in situ observations, J. Geophys. Res., 104, 30 463–30 480, 1999b.

Volz-Thomas, A., Berg, M., Heil, T., Houben, N., Lerner, A., Petrick, W., Raak, D., and Päetz, H.-W.: Measurements of total odd nitrogen (NO$_y$) aboard MOZAIC in-service aircraft: instrument design, operation and performance, Atmos. Chem. Phys., 5, 583–595, 2005.

von Glasow, R., von Kuhlmann, R., Lawrence, M. G., Platt, U., and Crutzen, P.J.: Impact of reactive bromine chemistry in the troposphere, Atmos. Chem. Phys., 4, 2481–2497, 2002.

Weinheimer, A. J., Walega, J. G., Ridley, B. A., Gary, B. L., Blake, D. R., Blake, N. J., Rowland, F. S., Sache, G. W., Anderson, B. E., and Collins, J. E.: Meridional distributions of NO$_x$, NO$_y$, and other species in the lower stratosphere and upper troposphere during AASE II, Geophys. Res. Lett., 21, 2583–2586, 1994.

Wernli, H. and Bourqui, M.: A Lagrangian "1-year climatology" of (deep) cross tropopause exchange in the extratropical Northern Hemisphere, J. Geophys. Res., 107, D1–D2, 4021, doi:10.1029/2001JD000812, 2002.

Ziereis, H., Schlager, H., Fischer, H., Feigl, C., Hoor, P., Marquardt, R., and Wagner, V.: Aircraft measurements of tracer correlations in the Arctic subvortex region during the Polar Stratospheric Aerosol Experiment (POLSTAR), J. Geophys. Res., 105, 24 305–24 313, 2000.